Aus der Universitätsklinik für Allgemeine, Viszeral- und
Transplantationschirurgie Tübingen

Soft liver phantom with a hollow biliary system

**Inaugural-Dissertation
zur Erlangung des Doktorgrades
der Medizin**

**der Medizinischen Fakultät
der Eberhard Karls Universität
zu Tübingen**

vorgelegt von

Tan, Xiangzhou

2022

Table of Contents

Index of figures and tables

List of figures

List of tables

IV

Nomenclature

3D	3-dimension
ABS	Acrylonitrile butadiene styrene
ACGME	The Accreditation Council for Graduate Medical Education
AR	Augmented reality
C	Celsius
CBD	Common bile duct
CD	Cystic duct
CDS	Choledochoduodenostomy
CHD	Common hepatic duct
CT	Computer tomography
EMR	Endoscopic mucosal resection
EPU	Elastomeric polyurethane
ERCP	Endoscopic retrograde cholangio-pancreatography
ESD	Endoscopic submucosal dissection
EUS	Endoscopic ultrasound
EUS-BD	Endoscopic ultrasound biliary drainage
FDM	Fused Deposition Modelling
Fig.	Figure
FPU	Flexible polyurethane
GBD	Gallbladder drainage
GI	Gastrointestinal/Gastrointestine
HD	High resolution
HGS	Hepaticogastrostomy
hrs/h	Hour(s)
HU	Hounsfield unit
IHD	Intrahepatic duct
kPa	Kilopascal
LC	Laparoscopic cholecystectomy
LHD	Left hepatic duct
mm	Millimeter
MRI	Magnetic resonance imaging

ms	Millisecond
MSD	Medial segmental duct
PA12	Polyamide 12
PAA	Polyacrylamide
PEBA	Polyether block amid
POC	Direct peroral cholangioscopy
PTC	Percutaneous transhepatic cholangiography
PTCD	Percutaneous transhepatic cholangiodrainage
PTCs	Percutaneous transhepatic cholangioscopy
PTLC	Peroral transluminal cholangioscopy
PVA	Polyvinyl alcohol
PVA-C	Polyvinyl alcohol
PVC	Polyvinyl chloride
RHD	Right hepatic duct
RHD	Right hepatic duct
RMSE	Root mean square error
s	second(s)
SD	Standard deviation
SLA	Stereolithography
SLS	Selective laser sintering
SOS	Speed of sound
stl	Stereolithography file
TCP	Flexible thermoplastic composite pipe
TPE	Flexible thermoplastic elastomers
TPU	Flexible thermoplastic polyurethane
USA/US	United States of America
UV	Ultraviolet
VR	Virtual reality
wt %	Weight percentage
μm	Micrometer
Ω	Ohm

1. <u>Introduction</u>

1.1. <u>The prevalence of liver disease and the need for the training of transhepatic interventional procedures</u>

The Liver is a vital organ in the digestive system, which involved numerous physiological processes, including lipid and cholesterol homeostasis (Chiang, 2013, Groen et al., 2014, Sica et al., 2014), immune response (Campisano et al., 2019, Heymann et al., 2015, Nakagaki et al., 2018), macronutrient metabolism (Bowman et al., 2019, Mu et al., 2019), blood-volume regulation (Bankir et al., 2017, Trefts et al., 2017), and the degradation of xenobiotic compounds (Manzanares et al., 2015, Ookhtens et al., 1998), and so on. Besides, the liver also participates in the process of glycometabolism, via storing glucose in the form of glycogen (Xiang et al., 2018, Yao et al., 2018). Liver diseases are considered the secondary leading cause of fatality amongst the whole digestive diseases in the United States (Everhart et al., 2009). The burden of liver disease in Europe is the largest in the world, and the burden is expected to continuously increase in many countries (Pimpin et al., 2018). The potential risk factors that cause the occurrence of liver diseases include extra alcohol consumption, viral hepatitis, and obesity.

The bile duct is one of the most important components and accessories of the liver organ. The main function of the biliary tract is to drain the bile juice that is secreted from the liver parenchyma into the intestine (major duodenal papilla) (Banales et al., 2019, Boyer, 2013). The most common biliary diseases consist of cholangitis, traumatic injury, and hepatocholangioma (Bergquist et al., 2015, Thompson et al., 2013, Yokoda et al., 2019). The occurrence of these diseases is possibly accompanied by certain complications, such as obstructions of the bile duct, bile leaks, and biliary infection. With the development of endoscopy and interventional therapy, these diseases and complications are more frequently diagnosed or treated via transhepatic interventional procedures.

The interventional procedures involving intrahepatic duct include but not limited to

- Endoscopic retrograde cholangiopancreatography (ERCP), a procedure that incorporates the utilization of fluoroscopy and endoscopy to diagnose or treat certain problems in the biliary or pancreatic system. The physician intubates a scope from mouth to duodenum, and then injects a contrast agent into the bile ducts to visualize the biliary and pancreatic system on the radiograph (Aabakken, 2012, Laugier et al., 2011).

- Percutaneous transhepatic cholangiodrainage (PTCD), a procedure that combines fluoroscopy and ultrasound guidance to alleviate intrabiliary pressure, which causes by biliary obstruction. The procedural route penetrates the abdominal skin, hepatic parenchyma, and finally into the bile duct. A stent or tube is placed in the liver with the guidance of ultrasound, to drain the bile juice to the small intestine or a collection bag outside of the body (Ogura et al., 2016, Radosa et al., 2019).

- Direct peroral cholangioscopy (POC), an endoscopic procedure that utilizes an ultra-slim endoscope directly into the biliary tract through a natural orifice. The procedure allows endoscopists to directly visualize the biliary mucosa and lumen (Itoi et al., 2011, Parsi, 2011).

- Endoscopic ultrasound biliary drainage (EUS-BD), a procedure that is developed as a novel alternative approach for failed ERCP. There are two main routes, including transgastric and transduodenal approaches. Three common EUS-BD procedures have been reported, i.e., EUS-guided hepaticogastrostomy (HGS), choledochoduodenostomy (CDS), and gallbladder drainage (GBD) (Chavalitdhamrong et al., 2012, Minaga et al., 2018).

These interventional procedures are becoming more and more popular (Kedia et al., 2013, Thomson et al., 2018). For instance, the annual number of ERCPs in the United States is projected to be over 45,000, with the use of therapeutic ERCPs steadily increasing (Kozarek, 2017, NIH_Consensus, 2002). In general, interventional techniques offer a less invasive method of treating patients, with a lower surgical risk and a shorter hospital stay than open surgery, such as, surgical bile duct exploration (Mukai et al., 2017, Parsi, 2011).

The interventional procedures are normally performed by experienced endoscopists, since these procedures are difficult to learn due to the following reasons (Cappell et al., 2019):

- There is a high risk of complications, including pancreatitis, bile leaks, biliary infection, and hemobilia;

- Interventional procedures require high-level technical expertise, as well as professional knowledge;

- There are few training opportunities available, most of which are in academic medical centers or tertiary hospitals.

Furthermore, the training of the transhepatic interventional procedures cannot meet the growing demand. For example, the majority of training centers do not have an adequate number of ERCP practices for the internship training (Leung et al., 2011). As demonstrated in previous studies, a minimum of 200 ERCPs was suggested for the competency acquisition (Garcia-Cano, 2007). 74% of GI residents intended to perform ERCP despite feeling that their ERCP training was insufficient (Kowalski et al., 2003).

Therefore, the training for the interventional procedure is needed to meet the repetition threshold.

1.2. The history and development of surgical training

In the middle ages, surgeons were regarded as "Mister" because of the trade of "barber-surgeon" (Popa et al., 2018). In this era, barber-surgeon worked for a wide range of tasks from haircutting to limbs amputating. This kind of surgeon did not require formal training, qualification, or degree. It can be expected that surgical mortality during the period was significantly high as a result of infection and bleeding (Akhaddar, 2018).

However, surgical training has been greatly evolved in the millennia since the inception of the art of surgery. The first small steps in the long history of surgical training are promoting training in the craft of surgery and transforming it from part-time to the profession. After being aware of medicine as an independent field, academic surgeons began to appear in order to differentiate from barber

surgeons that received sparse training or even no training. Around the early thirteenth century, the college de Saint Come was established in Paris and firstly identified the academic surgeon as surgeons of the long robe, specifically refers to those who had attended the university or had training (Wanjek, 2003). In the meantime, the barber-surgeons were recognized as surgeons of the short robe (Franzese et al., 2007, Wanjek, 2003). Subsequently, a school was built in France by the brotherhoods of St. Domains and St. Cosmos in the middle of the thirteenth century, to systematically teach barbers in surgical procedures (Franzese et al., 2007, Wanjek, 2003).

In the mid-sixteenth century, a standard apprenticeship approach became one of the most well-established and common methods for surgical training and education (Dobson et al., 1979, Majno, 1975, Young, 1890). The apprenticeship would have a long period of five to seven years, and it could begin in early childhood at the age of twelve or thirteen. Additionally, further education was accessible in the way of journeyman ships, either the same or different masters were in charge of the teaching of every surgeon. However, this further education was not mandatory for the surgical practice. In the beginning, the apprenticeship was proceeded simply with a non-structural arrangement, and normally within families and friends. The surgical apprenticeship was then developed more formally with organized arrangements and some formal principles. For instance, the surgical master had an obligation to instruct and teach, and they were obliged not to transfer their prentice to another surgical master in Edinburgh during the sixteenth century (Creswell, 1926). Since then, this time-honored approach has been the standard of surgical education. And it has been proved to be practical, and remains to the present. Generally speaking, apprentices were taught surgical procedures via direct observation in the operating room or the clinical examination setting. And students were then imitating the surgical procedures followed the actions of an experienced master (Dunnington, 1996). A famous adage "see one, do one, and teach one" came from this way, which accompanies personal experience and instruction too (Walter, 2006). To some degree, the introduction of an apprenticeship model significantly promotes surgical training and education. The students were instructed by the medical experiences of an experienced master, and trainees imitated and repeated the surgical techniques under the

guidance of their mentor. The most significant advantage is that the surgical knowledge and skills were learned by examples and instructions instead of error or trial. However, there was still no systematic guideline or standardization to educate or train the apprentices. With the expansion of masters who built competing "schools of surgery", the apprenticeship model somehow became the "cult of the individual" (Hamdorf et al., 2000).

In the nineteenth century, surgical training and education started to shift from the apprenticeship models to more structured and formalized training models. The approach is also very popular in recent education models to train surgical residents. The popularization of the structured and formalized training model was largely because of the proposal of Dr. Willian Osler and the promotion of Dr. William Halstead (Nguyen et al., 2006, Rankin, 2006). In 1890, Osler came up with this approach and proposed it to the Board of Trustees at the Johns Hopkins Hospital. Halstead was hearty to adopted it and without any hesitations (Rankin, 2006). It has to be stressed out that Halsted played an important role in the history of surgical education. He set up a school for surgical training, which gave priority to the safety during the surgery, i.e., meticulous hemostasis and cautious tissue handling (Robert et al., 1983). Also, as mentioned previously, he greatly promoted the popularity of resident training in the United States. In 1904, Halstead presented a remarkable lecture at Yale on the topic of surgical training, that suggested the adoption of the German residency training model. This model allowed medical students to receive increasing responsibilities with each boosting resident year (Grillo, 1999, Nguyen et al., 2006). And the training model improved structure and standardization during the surgical training. The "pyramid" structure was also introduced in the residential training, which means the number of surgical candidates would be decreased every residency year and a single chief resident would stay after the graduation year (Nguyen et al., 2006). Finally, the proposal of residency programs and fellowships was approved by the American Medical Association House of Delegates in 1928 (Hamdorf et al., 2000). The embryonic form of the surgical educational training programs and residency educational models in the United States has been formed and retains to this day.

At the present, surgical training and education are quite versatile. With the rising

consciousness for the significance of surgical education, more and more approaches have been emerged to improve the surgical techniques and knowledge, for example, workshop and seminar, simulation-based training, conference, remote education, clinical further education/visiting, and so on. There is no doubt that the appearance of these methods for surgical training provides a promising future for surgical education. The history of surgical training and education is summarized in Figure 1.
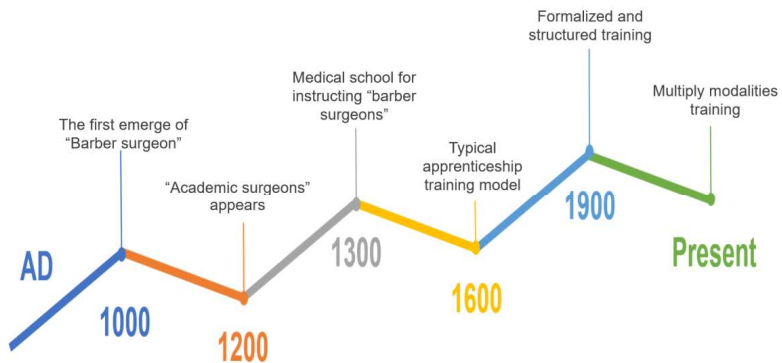
Figure 1. A brief summary of the history of surgical training and education.

However, the key to improve surgical competency is practice (Kotsis et al., 2013, Rui et al., 2018). Plenty of studies reported that increasing the volume is significantly correlated with the performance improvement of surgeons (Birkmeyer et al., 2003, Ericsson, 2008, Sosa et al., 1998, Stavrakis et al., 2007). In addition to that, the increasing time in deliberate practice is also very important rather than tremendous repetition, so as to achieve the expert level (Ericsson, 1996, Halm et al., 2002). There are two basic approaches for actualizing deliberate practice, including continually setting up new objectives and higher performance levels, searching out training circumstances to achieve the goals. These approaches mainly avoid automated repetition that extra experiences do not convert to improve surgical performance (Ericsson, 2008). The four steps to achieve deliberate practice are presented in Table 1.

Table 1. The conditions to achieve deliberate practice. (Ericsson, 2008)

Four Steps of Deliberate Practice:
1. Have a task with a well-defined goal
2. Be motivated to improve
3. Be provided with immediate feedback
4. Be provided with ample opportunities for repetition and gradual refinements of performance

The most useful method for safely and effectively improving medical professionals' capabilities is through the use of a simulation-based training model. Numerous studies indicate that surgical simulators can help improve the early learning curves, provide dedicated learning environments, and help avoid patient discomfort or even potential adverse events (Waschke et al., 2018). The Accreditation Council for Graduate Medical Education (ACGME) demonstrates that simulations and skills laboratories are recommended in the resources of resident education (ACGME, 2008). According to the study of Issenberg et al, patients are also happier to allow surgical students to perform some medical procedures on them after the surgical student received the simulation-based training (Graber et al., 2005). Furthermore, a meta-analysis points out that the simulation-based training combined with deliberate practice is more significantly effective in the acquisition of clinical skills (p-value< 0.001), compared to the traditional apprenticeship training model – "see one, do one, and teach one" (McGaghie et al., 2011).

1.3. The types of simulators

There is an increasing tendency of the adoption and utilization of simulators as part of surgical training, credentialing, and privileging (Desser, 2007, Singh et al., 2014). In the aviation industry, simulators have been an indispensable tool for the daily training and competency assessment of civilian or military pilots (Lei et al., 2021, Lowther et al., 2021, Singh et al., 2014). In gastroenterology and hepatology, simulation for training physicians has been used mainly for the

acquisition of new techniques, e.g., laparoscopic cholecystectomy (LC), endoscopic therapeutic procedures, interventional radiology, and so on (Dawe et al., 2014, Ostergaard et al., 2016, Sujka et al., 2018). There is a wide variety of surgical simulators available for the training of physicians, including mechanical simulators, live animal models, ex vivo models, and virtual reality (VR) models (van der Wiel et al., 2016).

1.3.1. Mechanical models

Mechanical models, i.e., physical simulators, are using various non-tissue materials to resemble anatomic structures. Both part-task simulators and organ phantoms belong to the mechanical models (van der Wiel et al., 2016).

The part-task simulators give priority to some particular tasks that can be practiced and learned, rather than attempting to acquire actual procedural experience. For example, the skills for performing endoscopy are divided into different components, including tip control, torque, insertion, and reduction (Waschke et al., 2018). Figure 2 shows a part-task simulator for the improvement of endoscopic skills. A recent study demonstrated that the part-task models quickly and significantly improve the skills of novice, and it can convert to clinical benefits in the early stage of the learning period (Waschke et al., 2018).
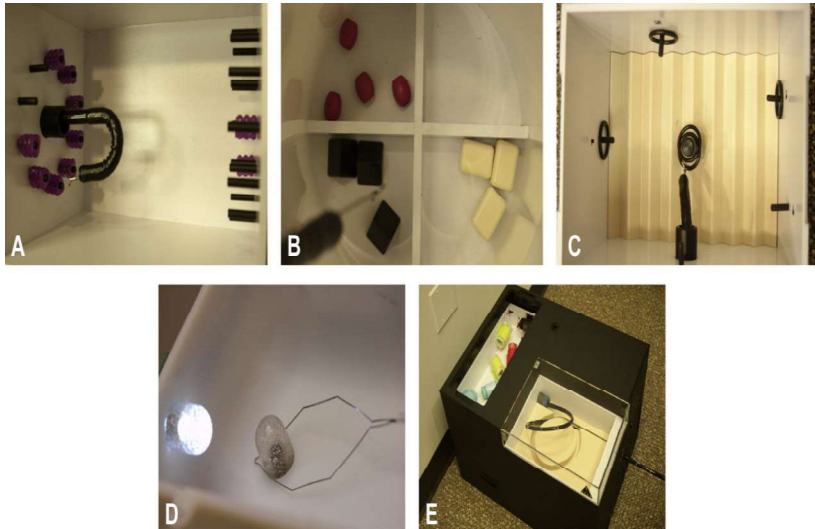
Figure 2. Part-task simulator for endoscopic skills. A. Endoscopic retroflexion; B. Endoscopic knob control; C. Endoscopic torque; D. Endoscopic polypectomy; E. Endoscopic navigation/Loop reduction. (Jirapinyo et al., 2015)

The organ phantom models or box models are also used extensively in medical education. This kind of phantom is the most basic and inexpensive of the simulator, which is suitable for basic training or didactical training. It shows a good abstract anatomy demonstration, real-time physical interactions, and long-term durability (Choi et al., 2020, King et al., 2016). Some organ phantoms, such as the brain phantom (Forte et al., 2016), the cardiac phantom (Gosline et al., 2012, Parsi, 2011), and the gastrointestinal (GI) phantom (Garbin et al., 2019) have been constructed for advanced surgical training and robot testing. Furthermore, the structures of organs and the pathological lesions are able to be completely copied with the development of 3D printing technology (Dhir et al., 2015, Holt et al., 2015). Although the simulation of tissue properties is still a problem, a wide variety of polymers and hydrogel materials provide a good selection for the simulation of different biological tissues with different mechanical, acoustic, and electrical properties.

1.3.2. Live animal simulator

Live animal simulators exhibit great advantages in biological tissue. The physiological characteristics, including secretion, respiratory movement, and bleeding, resemble the conditions that encounter in clinical practice. Several therapeutic procedures, e.g., hemostasis, electrotomy, coagulotomy, are able to perform in the animal simulator. A live swine model for endoscopic training is shown in Figure 3. Swine is one of the most commonly-used live animal simulators for surgical training, even though other animal simulators also have been described in various studies (Desilets et al., 2011, Falkenstein et al., 1974). However, animal simulators possess significant disadvantages, including inconsistency with human anatomic structures, inability to be reused, non-standard, and expensive, as well as the requirement for veterinary support (Adams et al., 2017, Waschke et al., 2018). Moreover, ethical issues must be resolved in the light of ethical principles and the local law. For example, animal experiments with dogs, cats, and non-human primates are prohibited in the European Union, except for the animals that have been bred for this purpose, which is quoted from Directive 2010/63/EU of the European Parliament (Parra-Blanco et al., 2013). The restrictions for living primate species are even severer.
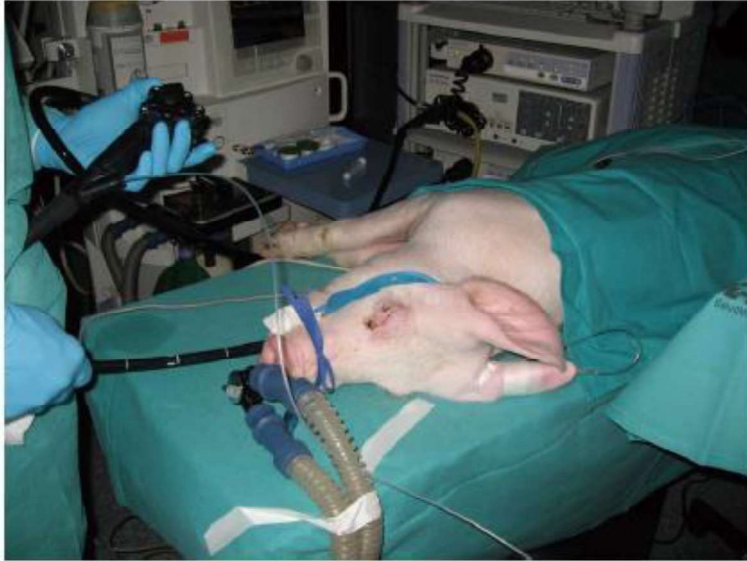
Figure 3. Live swine simulator for endoscopic training. (Herreros de Tejada, 2014)

1.3.3. Ex vivo simulators or hybrid simulators

To overcome some of the disadvantages of live animal simulators, hybrid or ex vivo simulators combine a plastic outer shell or torso with detached animal organs. These models have been utilized frequently in recent years (Ahn et al., 2016). The part of animal tissue is placed in a mechanical device. Other attachments and devices are also added, which depend on the content of training, such as a pump system for fluid perfusion. The example of an ex vivo simulator is presented in Figure 4 (Jung et al., 2013). A porcine or bovine organ with arteries or artificial tubes sewn in the mucosa is well-prepared to simulate upper gastrointestinal bleeding. The model is possible to train endoscopic advanced procedures, including endoscopic mucosal resection (EMR), endoscopic submucosal dissection (ESD), Endoscopic clipping, and so on (Palter et al., 2011, Thomson et al., 2018).

The primary advantages of hybrid simulators are that the biological tissue has similar properties to human tissue. The ex vivo simulator, therefore, has the

possibility of practicing a bunch of therapeutic maneuvers with real accessories that are used in the hospital. Nevertheless, the devitalized organs perform worse than live animal models and it can make some procedures like variceal banding or ligation, mucosal resection, and submucosal injection harder to perform (Tamada et al., 1999, Velazquez-Avina et al., 2014).

Figure 4. Ex vivo porcine stomach simulator. (Jung et al., 2013)

1.3.4. Virtual simulator

Virtual simulators are one kind of equipment that rebuilds a virtual reality on a computer screen or cyberspace to train cognitive and technical skills under diverse conditions. The virtual simulator incorporates both visual and haptic interfaces, attempting to resemble the clinical environments. Many studies reported significant benefits in the acquisition of skills and surgical efficiency (Waschke et al., 2018). The effects on training novice endoscopists, especially in the initial clinical cases, are the most pronounced (Ferlitsch et al., 2010, Koch et al., 2015). Besides, virtual simulators provide an objective assessment of performances, e.g., procedural completion, the total time of the whole examination, and the ability to handle bleeding. The feedback of virtual simulators can function as a tutor to give real-time feedback and identify the deficiencies of the trainees. Meanwhile, it is also possible for the realization of the credentialing process via customizing benchmarks in the simulators.

There are several commercially available VR simulators. The virtual simulators in the field of laparoscopy include CAE LAPVR simulator (CAE healthcare, Montreal Quebec, Canada), LAP Mentor (3D systems, Littleton, United States), LAP-X (Medical-X, Rotterdam, Netherlands), and LAPSIM (Surgical Science, Gothenburg, Sweden), and so on (Huber et al., 2018, Shanmugan et al., 2014, Wynn et al., 2018, Yiannakopoulou et al., 2015). Figure 5 exhibits the product LAP Mentor from 3D systems company for the training of laparoscopic cholecystectomy (Ayodeji et al., 2007). The virtual simulators come with replica laparoscopes and various tools that resemble different devices, such as graspers, scissors, staplers, which depends on the chosen scenario. There are sensors inside the system to respond to the user's operation. Force or haptic feedback is also available to simulate the resistance during the procedure.

Figure 5. Virtual simulator manufactured by 3D systems/Simbionix LAP Mentor. (Ayodeji et al., 2007).

These manufacturers also provide endoscopic virtual simulators (Ferlitsch et al., 2002, Ferlitsch et al., 2010, Khan et al., 2018, Khan et al., 2019). The details of modules and costs for the endoscopic virtual simulators are listed in Table 2. All these virtual simulators have modules of upper GI bleeding, colonoscopy, and sigmoidoscopy, and so on. And these platforms are possible to intubate to the

cecum, perform loop reduction, hemostasis, and polypectomy, and so on. The insertions of accessories, e.g., snare and forceps, are also applicable. Endoscopic retrograde cholangiopancreatography (ERCP) is available in some certain virtual simulators, including Endo VR, GI mentor, and Endosim, while therapeutic ERCP only exists in the GI mentor system. Furthermore, the GI mentor platform has a diagnostic EUS module with linear and radial probes. Some advanced endoscopic procedures, such as EMR and ESD, have not been found on the market yet. The prices of virtual simulators are considerably expensive, ranging from $ 49,950 to $134,000.

Table 2. Virtual reality simulators for endoscopy. (Committee et al., 2019)

	Simulator			
	ENDO VR	**GI Mentor**	**Endo-X**	**Endosim**
Manufacturer	CAE HealthCare	3D Systems	Medical-X	Surgical Science
Monitors (numbers of monitors)	Yes (2)	Yes (1)	Yes (2)	Yes (2)
Cart	Yes	Yes	Yes	Yes
Integrated keyboard	Yes	Yes	Yes	Yes
Colonoscopy [a]	Yes	Yes	Yes	Yes
Sigmoidoscopy	Yes	Yes	Yes	Yes
EMR	No	No	No	No
Endoscopic submucosal dissection (ESD)	No	No	No	No
Upper GI bleeding [b]	Yes	Yes	Yes	Yes
ERCP [c]	Diagnostic only	Diagnostic and therapeutic	No	Diagnostic only
EUS [d]	No	Yes, diagnostic	No	No
Trainee feedback	Yes	Yes	Yes	Yes
List price	$119,600	$72,000-$134,000	$49,950	$60,000-$132,000

a Colonoscopy module includes advancement to cecum, snare polypectomy, forceps biopsy, and loop management
b Upper GI bleeding modules include clip placement and coagulation for control of bleeding
c Diagnostic ERCP modules include cannulation, contrast injection, and cholangiogram interpretation. Therapeutic ERCP modules include sphincterotomy and stent placement
d Diagnostic EUS modules include radial and linear imaging

Although virtual simulators are expensive, they can be used repeatedly and no dedicated equipment is required, such as laparoscope and endoscope. And the modules in the platform can be updated to adapt to newly developed modules and procedures. However, virtual models provide limited haptic feedbacks to

trainees, making the training scene nonrealistic. Moreover, there is no physical interaction with real surgical tools too, which compromises the training experience (Kunert et al., 2020).

To sum up, different types of simulators have both advantages and disadvantages. Organ phantoms (Kenngott et al., 2015) exhibit great advantages in durability, cost efficiency, and no involvements of ethical issues. It remains a challenge to establish a high-fidelity artificial organ simulator with detailed anatomic structures, soft properties material, vivid imaging results, and the ability to provide trainees with quantitative feedback on surgical performance. However, the emergence of fully-fledged 3D printing technology, e.g., Fused Deposition Modelling (FDM), Selective laser sintering (SLS), Stereolithography (SLA), has made it possible to fabricate a fully 3D organ phantom with high resolution, accurate anatomy details (Kong et al., 2016, Lin et al., 2018, van Noort, 2012). Meanwhile, the extension of printing materials also provides different possibilities for different phantoms with different mechanical properties, which enables the fabrication of complex structures (Adams et al., 2017, Garcia-Cano, 2007). Our previous work combined soft materials molding technologies and advanced 3D printing to establish realistic organ phantoms for medical training, such as a gastrointestinal interventional phantom (Grund et al., 2012), a soft kidney phantom (Adams et al., 2017), and a resectable prostate phantom (Choi et al., 2020). These technical advancements enable the fabrication of highly accurate organ phantoms using soft biomimetic materials.

1.4. Current research status of the liver phantom

To date, several liver phantoms have been made for surgical planning or simulation. The details of these phantoms are summarized below.

The important anatomical structures in some liver phantoms, including the hepatic artery, portal vein, patient-specific tumors, were fabricated by the 3D printing techniques based on the acquired imaging data from CT, magnetic resonance imaging (MRI), and cholangiography (Madurska et al., 2017, Pacioni et al., 2015). Nevertheless, these liver phantoms lack hollow inner structures such

as the biliary system, which is of significant importance concerning the transhepatic interventional simulation. Besides, most of them are made of hard plastic materials, compromising the haptic feedback during the surgical simulation (Javan et al., 2018, Madurska et al., 2017, Pacioni et al., 2015, Yang et al., 2018). Figure 6 shows the 3D printed liver models by Madurska et al (Madurska et al., 2017).
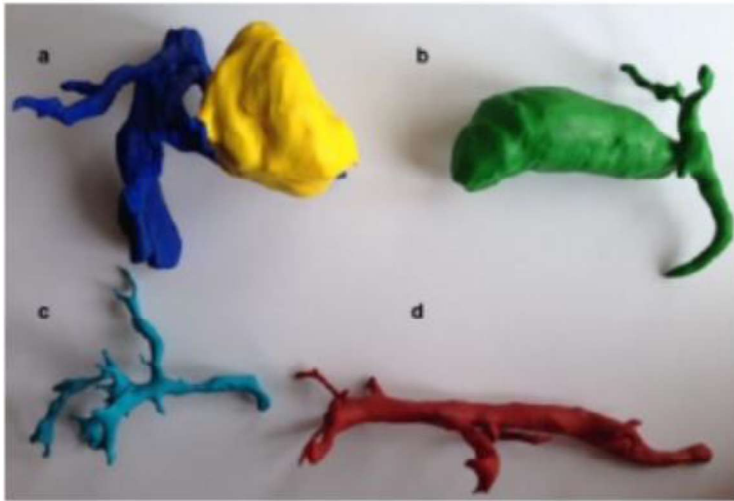
Figure 6. 3D printed hepatic models for surgical planning. a, Portal veins and hepatic tumor; b, Gallbladder and the corresponding biliary tree; c, Portal vein and its branches; d, Hepatic artery. (Madurska et al., 2017)

In 2015, Dhir et al. presented a novel ex vivo liver model for the simulation of endoscopic ultrasound-guided biliary drainage (EUS-BD) (Dhir et al., 2015). The hybrid liver phantoms include a plastic bile duct and ex vivo animal tissue. The bile duct was printed using polycarbonate by a 3D stereolithography system (3D systems, Rock Hill, SC). The liver parenchyma was resembled by porcine liver tissues. The phantom is applicable for several examinations, including x-ray, ultrasound. However, the anatomy of the liver and bile ducts, as well as their location, are underrepresented. And the imaging results on the ultrasound were not well presented. Figure 7 exhibits the prototype of the liver phantom for the interventional simulation.
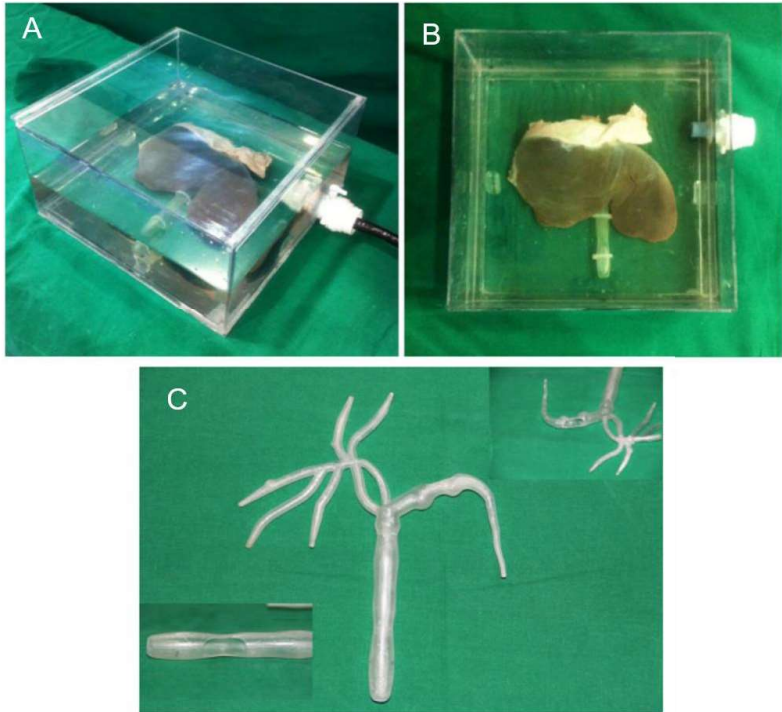
Figure 7. An ex vivo liver phantom for the training of endoscopic ultrasound-guided biliary drainage (EUS-BD). A, B different side view of the liver phantom; C, 3D printed biliary tract. (Dhir et al., 2015)

Tang et al. created a liver simulator for the examination of choledochoscopy in 2018 (Tang et al., 2018). The model was fabricated using 3D printing technology. An electromagnetic sensor was installed in the working channel of the choledochoscope to track the movement of the scope. Finally, an augmented reality (AR) system was established to navigate the choledochoscopy. The model depicts the biliary tract anatomically and accurately, but lacking of the surrounding liver precludes the use for transhepatic interventions or ultrasound-based procedures. Figure 8 shows the details of the liver model made by Tang et al.
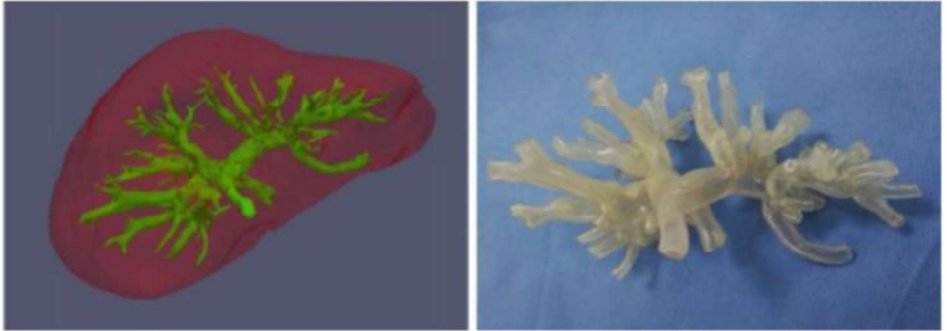
Figure 8. The 3D virtual liver model (a) and the model of intrahepatic biliary ducts (b). (Tang et al., 2018)

To our knowledge, there has not yet been a report of an anatomically accurate soft liver mechanical simulator obsesses both the hollow biliary system and the surrounding hepatic parenchyma.

1.5. Aim of the thesis

As we mentioned above, the medical training regarding transhepatic interventional procedures and surgery are highly demanding and hindered due to the technical difficulties, the high risks of procedural complications, rare accessibility in clinical practices, and so on. However, these interventional procedures have gained increasing acceptance and begun to be widely used. The requirement for developing a liver phantom for the training of such a procedure is urgently needed. Although there are several available liver phantoms in the research studies, the deficiencies of these liver phantoms, e.g., unrealistic anatomical structures, plastic-like haptic feedback, ethical issues, are not allowed for widespread use in transhepatic interventional training. The design and development of a soft liver phantom that is used for the training of transhepatic interventional procedures are of significant importance. Therefore, a novel, universal liver phantom that is applicable for certain examinations, including endoscopy, radiology, ultrasound, is developed for the training of transhepatic interventional procedures. To meet these requirements of the

training purposes, several characteristics in the liver phantom should be addressed during the materials selection and manufacturing process:

✧ Accurate anatomic structures: the recognition of anatomical landmarks is essential for the success rate of surgical procedures. The biliary tract's shape and location in the liver are critical in transhepatic interventional procedures. Besides, the shape of the liver also helps to localize the bile duct with the assistance of an imaging system.

✧ Realistic appearances: to some extent, the fidelity of the simulators affects the performance of medical training. The basis of deliberate training is adequate degree of realism.

✧ Analogous mechanical properties of human tissues: The simulator's haptic feedback is highly dependent on the material's material properties, such as elastic modulus and hardness. During interventional procedures, there are frequent interfaces between physicians, equipment, and tissue. The haptic feedback becomes particularly important especially in the training of advanced interventional procedures.

✧ The ability for ultrasound imaging: generally speaking, the interventional procedure involves the localization of the biliary tract undergoing ultrasound, as well as the guidance of puncture needles. Therefore, the ability for exposing the bile duct undergoing ultrasound examination is critical.

✧ The ability for radiologic imaging: choledochography is one of the most important diagnostic tools for biliary disease. The therapeutic procedures, e.g., stent placement, balloon dilation, are performed under the assistance of radiology. Hence, the ability for radiologic imaging is a prerequisite characteristic of the liver phantom for interventional training.

✧ The ability for endoscopic imaging: with the development of ultra-slim endoscopes, the use of cholangioscopy becomes more and more common. The possibility for cholangioscopic training is also an

important characteristic.

✧ The hollow biliary system: most procedures during the transhepatic interventions, including the insertion of guidewires, stent placement, needle puncture, and balloon dilation, are performed in the biliary system. The ductal structures in the liver phantom are an indispensable condition.

✧ The assessment of procedural performance: A timely assessment of the interventional procedures is critical for achieving deliberate training. Several parameters are very important to assess the performance of the interventional procedures, e.g., whether the transhepatic needle punctures exactly in the bile duct, or which segmental ducts does the needle pierces in.

✧ Durability: interventional procedures normally base on the transhepatic puncture procedures. Repeatedly puncturing is required for the interventional training. The design of the simulator should consider the durability property to ensure the service life.

✧ Inexpensive: The cost of the simulator is one of the most important considerations. The use of the simulator can be widely accepted only when the price of the simulator is acceptable.

The aim of the project was to create an intervenable model of an anatomically correct liver organ with included intra- and extrahepatic bile ducts according to the above requirements.

2. Materials and Methods

2.1. The schematics of fabricating a soft liver phantom that possesses a hollow biliary system for the purpose of training in hepatic intervention procedures

The project's schematics are shown in Figure 9. The goal is to create a soft liver organ phantom that possesses a hollow biliary system for the training in hepatic intervention procedures. Based on anatomic knowledges, a biliary system, including the intrahepatic duct and extrahepatic duct, was designed via 3D modeling software. A new fabrication method that combines 3D printing and molding was used to fabricate the liver phantom with a hollow biliary structure. Multiply imaging examinations were then applied to assess the fidelity of the liver phantom, including CT scan, endoscopy, and ultrasound. All of these examinations are common medical imaging techniques for hepatic diseases. Finally, a medical procedure, i.e., transhepatic puncture procedure, was simulated in the new phantom to assess the practical use. Meanwhile, a real-time needle tracking system for the quantitative evaluation of endoscopic procedures has been developed (Tan et al., 2021).
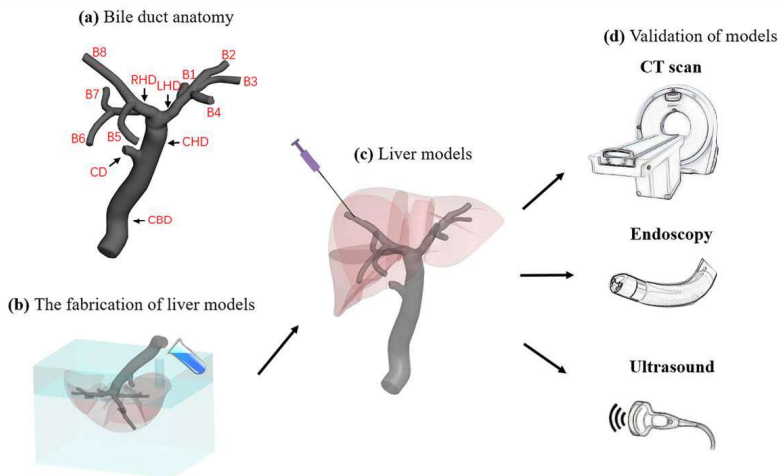
Figure 9. Schematics of the soft liver mechanical phantom possessed a hollow biliary system for the medical training. (a) the anatomic structure of the biliary system; (b) the

fabrication of the liver phantom by 3D printing and molding methods; (c) simulation of a transhepatic puncture procedure in the liver phantom; (d) the validation of the model via multi-modality medical imaging. CBD, common bile duct; CHD, common hepatic duct; CD, cystic duct; RHD, right hepatic duct; LHD, left hepatic duct; B1-B8, segmental duct. The picture is derived from a published article written by our groups. (Tan et al., 2021)

2.2. The design of the 3D digital liver model based on the liver anatomy

2.2.1. The anatomy of the liver and corresponding bile duct

Proficiency in the anatomy of the liver, especially the internal anatomy of the liver, is a prerequisite for a good hepatic surgeon. The detail of intrahepatic anatomy was mainly disclosed by a French surgeon and anatomist, called Claude Couinaud, who detailed his work in "*The Liver: Anatomic and Surgical Studies*" in 1957 (Abdel-Misih et al., 2010). His theory points out that hepatic functional anatomy relies on the vascular and biliary network rather than the external surface anatomy, which greatly improves the safety and possibilities of hepatic surgery (Abdel-Misih et al., 2010).

The Couinaud classification of hepatic segments divides the liver into eight distinct segments based on the presence of dual vessels, biliary drainage, and lymphatic drainage in each segment (Abdel-Misih et al., 2010). Each segment was assigned a Roman number (I to VIII), starting with the caudate lobe (I), followed by the left lateral superior segment (II), the left lateral inferior segment (III), the left medial segment (IV), the right anterior inferior segment (V), the right posterior inferior segment (VI), the right posterior superior segment (VII), and the right anterior superior segment (VIII) (Abdel-Misih et al., 2010). See Table 3 for more information (Abdel-Misih et al., 2010).

Table 3. The anatomy of hepatic segments

Lobes	Segments	"Couinaud" classification	Corresponding bile duct
Left lobe	Caudate lobe	I	B1
	Left lateral superior segment	II	B2
	Left lateral inferior segment	III	B3
	Left medial segment	IV	B4

Right lobe	Right anterior inferior segment	V	B5
	Right posterior inferior segment	VI	B6
	Right posterior superior segment	VII	B7
	Right anterior superior segment	VIII	B8

As illustrated in Figure 10, three hepatic veins run in three vertical planes to divide the liver into four segments. For example, the right hepatic vein divides the right lobe into right posterior (Segments VI/VII) and right anterior (Segments V/VIII) sections. The liver is divided into right and left lobes by the middle hepatic vein. Left lobe is divided into left lateral and left medial sections by the left hepatic vein. Meanwhile, a horizontal plane (the portal plane), through which the Glisson's capsule passes, divides each liver section into two segments, superior and inferior segments.
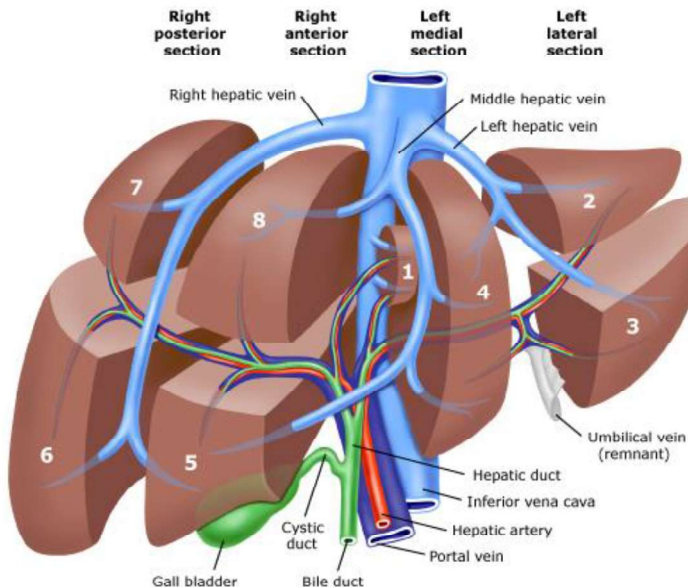
Figure 10. Hepatic functional anatomy based on vascular and biliary relationship. The image is taken from the website:
(https://ranzcrpart1.fandom.com/wiki/Abdomen:Solid_viscus:Couinaud_segments).

2.2.2. Design of the 3D digital liver model

The design of 3D digital model should fully consider the functional anatomy of the liver, especially the diameters, shape, and orientation of both normal and abnormal structures. After a literature review, the technical data of different bile ducts are summarized in Table 4.

Table 4. The technical data of normal and abnormal anatomic structure

Anatomical Name	Length	Diameter (Normal)	Diameter (Dilated)	Thickness (Normal)	Thickness (Disease)
Common bile duct	6-15 cm (Blidaru et al., 2010)	5.25(4-14) mm (Blidaru et al., 2010)	8-12 mm (mild) 12-16 mm (moderate) 16-20 mm (severe) >20 mm (extremely severe) (Lv et al., 2015)	1.0 mm (1.5 mm max) (Schulte et al., 1990)	2-5 mm (Schulte et al., 1990)
Cystic duct	2-4 cm (Sureka et al., 2016)	1-5 mm (Turner et al., 2001)	6-13 mm (Parulekar, 1989)	-	-
Common hepatic duct	6-8 cm (Hoeffel et al., 2006)	6-10 mm (Graham et al., 1980)	8.8 mm (5-20 mm) (Hoeffel et al., 2006)	0.94 mm (1.5 mm max) (Schulte et al., 1990)	0.8-5 mm (Schulte et al., 1990, Tamada et al., 1999)
Left (right) hepatic duct	-	3-4 mm (Blidaru et al., 2010)	5 mm (mild) 5-9 mm(moderate) >9 mm(severe) (Lv et al., 2015)	-	-
Lobar ducts	-	0.4-0.8 mm (Han et al., 2013)	-	-	-
Interlobular bile ducts	-	0.02-0.10 mm (Han et al., 2013)	-	-	-

According to the above data regarding the anatomical structures of the biliary tract, as well as medical experts' knowledge and experience, two 3D digital models of a biliary system for both normal and dilated bile duct were designed. Due to the significance of diameters of the bile ducts, the details of diameters in real patients and our phantom are presented in Table 5. The diameters of the segmental ducts, intrahepatic duct (left), intrahepatic duct (right), common hepatic duct, cystic duct, and common bile duct were set to 1 mm, 3 mm, 4 mm, 10 mm, 4 mm, and 11 mm, respectively, in the phantom of the normal case. And the diameters of the bile ducts in the phantom biliary dilation cases were set to replicate clinical biliary dilations, that is 6 mm, 8 mm, 10 mm, 18 mm, 8 mm, and 20 mm for the segmental ducts, intrahepatic duct (left), intrahepatic duct (right), common hepatic duct, cystic duct, and common bile duct, respectively (Dhir et al., 2015, Kozarek, 2017). Each segmental bile duct was localized corresponding to the anatomy of the liver segments. And Figure 11 and Figure 12 show the front-side view of the designed biliary tract (Tan et al., 2021).

Table 5. The design of bile duct's diameters in the different sites and cases

Site/Cases	Real human (mean/range, mm)	The phantom of normal case (mm)	The phantom of biliary dilation case (mm)
Common bile duct	5.3(4-14)	11	20
Cystic duct	1-5	4	8
Common hepatic duct	6-10	10	18
Left (right) hepatic duct	3-4	3-4	8-10
Lobar duct	0.4-0.8	7	10
Segmental duct	< 0.1	2~1	7~6
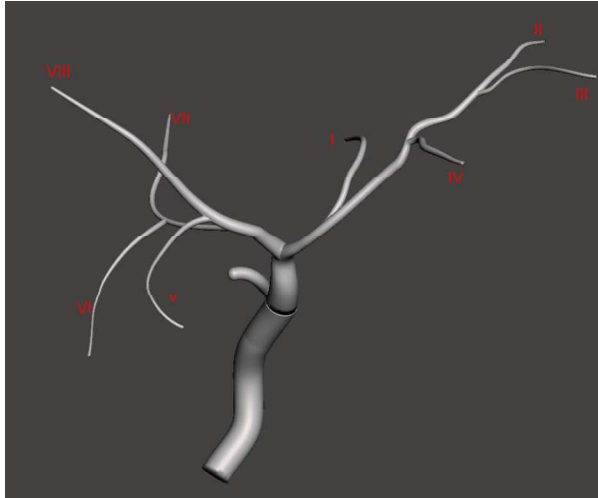
Figure 11. Design of the normal bile duct (from own recording).
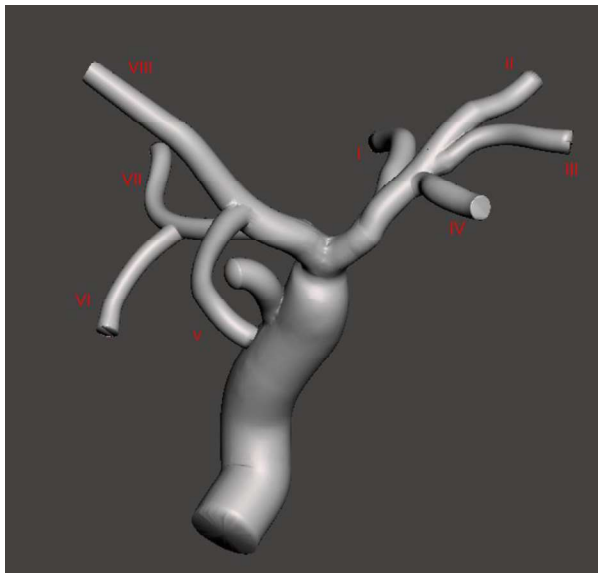
Figure 12. Design of the dilated bile duct (from own recording).

The 3D digital model of the outer shape of the liver was downloaded from an open

resource website (BodyParts3D, https://lifesciencedb.jp/bp3d/) and then customized for the current research. The original dataset's division of the liver segments was preserved, as illustrated in Figure 13 (Tan et al., 2021).
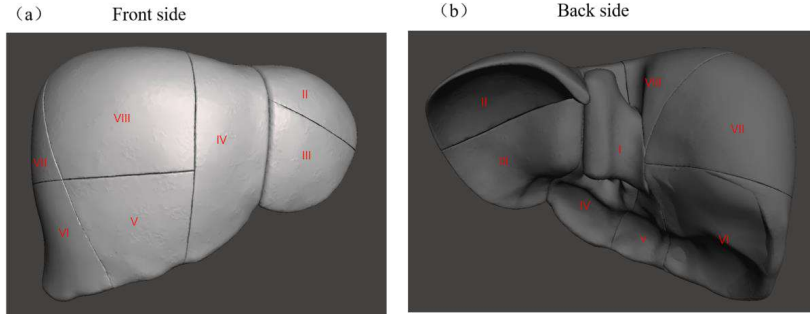
Figure 13. Design of the 3D model for the liver outer shape (from own recording).

SolidWorks software (Dassault Systèmes SE, France) was used to create the three-dimensional digital liver and biliary system models. Additionally, they were decreased to 80 percent size in all three dimensions using the Meshmixer software (Autodesk Meshmixer 3.5) to conserve 3D printing time and materials (Tan et al., 2021).

2.3. The fabrication of the liver phantom

2.3.1. The feasibility of the fabrication method

In this study, we used a new fabrication method to build a hollow structure in a soft model. The method is to use a transformable inner mold to create a complex hollow structure. As shown in Figure 14, a flexible inner mold can be transformed during the demolding process. After the removal of the inner mold, the complex hollow structure was left without destroying the inner mold and the resultant structure.
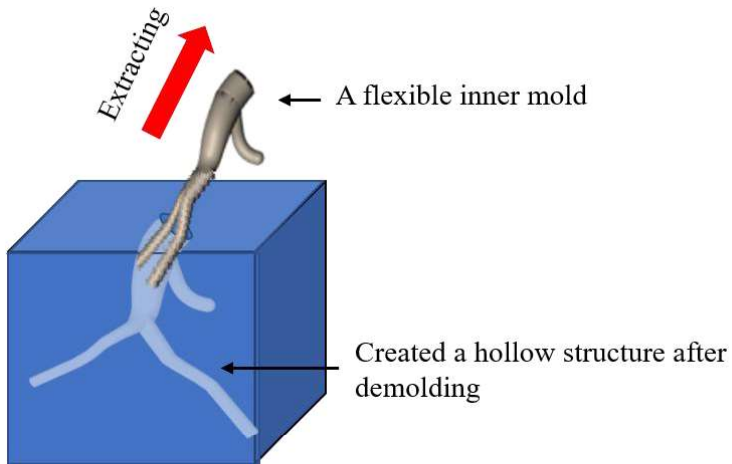
Figure 14.The theory of the fabrication method (from own recording).

2.3.2. The selection of 3D printing materials

To explore the most suitable 3D printing materials for the fabrication of inner molds, a simple 3D digital model was created (Figure 15). The reason for the selection was that the angle of the bifurcation between the left and right hepatic duct is relatively large, which means the deformation of the inner mold in this part is the highest, subsequently resulting in difficulties during the demolding process. If this part of the inner mold is not damaged during the demolding process, then the material is considered feasible for our fabrication approach.
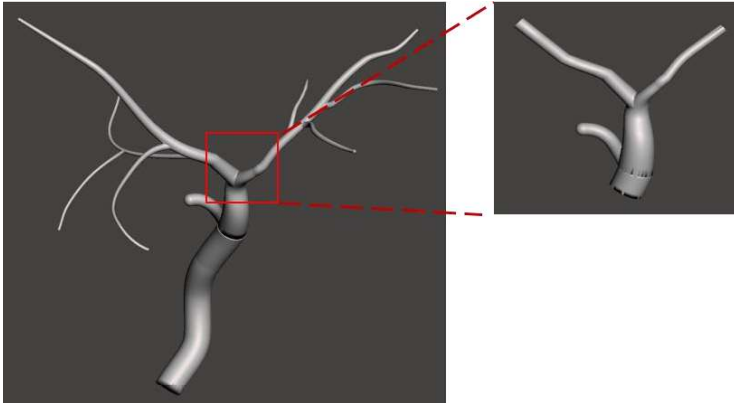
Figure 15. Design of small sample models for 3D printing material test (from own recording).

Four 3D printing materials were selected for the material test, including Tangoblack, FLEX9060-DM, FLEX9095-DM, and RGD8730-DM (Stratasys company), see details in Figure 16. Two sizes of the simple 3D digital model were printed using each of the above materials on a 3D printer for commercial use (Object 260 Connex, Stratasys). The diameters of the tip of the simple 3D digital model are 3~4 mm, 1~2 mm, respectively, which represented the size of the hepatic bile duct (3-4 mm), segmental bile duct (1-2 mm), respectively.
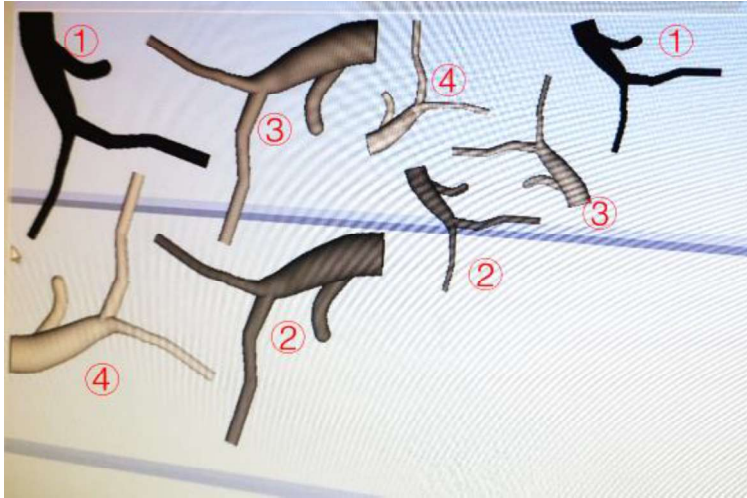
Figure 16. Eight samples for the materials test of inner mold (from own recording).

2.3.3. The selection of molding materials

According to the literature, organic phantoms are normally fabricated by hydrogel materials, due to their low costs and acoustic properties, i.e. echogenicity (D'Souza et al., 2001b). However, these hydrogel phantoms have a short life time with an estimated usable life of 2/3 years. Furthermore, their working life could even be shorter when they serve for the training of invasive surgeries, including biopsy and puncture procedures.

The selection of molding materials highly depends on the application of the phantom. In this study, we focus on the training of transhepatic puncture procedures, the durability and punctuality are the most important factors. Therefore, silicone polymers were used as basic material due to their durability and stability over time (Pacioni et al., 2015). But the silicone polymer is anechoic undergoing ultrasound scanning, which contradicts the iso-echogenicity of the hepatic parenchyma, see details in Figure 17.

Figure 17. The ultrasound imaging of a real human liver. The image is obtained from reference (NIH_Consensus, 2002)

To simulate the lifelike ultrasonic signal, some glass beads with different diameters were mixed with the silicone. A silicone polymer (Ecoflex 0020, Smooth-On, PA, USA) was selected because its mechanical properties (elastic modulus: ~60 kPa) is comparable to the parenchyma of the human liver (0.5 – 70 kPa) (Adams et al., 2017, Żmudzińska et al., 2018). Ecoflex 0020 was mixed via a glass rod in a volume ratio of 1:1 (Part A: Part B), different glass beads (φ= 600, 200,10 µm) were then mixed with silicone materials in a weight ratio of 10%, and the mixtures were placed in the oven for curing with 63 °C for 4 hrs, see the samples in Figure 18. The fabricated material was imaged using a medical ultrasonographic imaging system (LOGIO P6, GE Healthcare, Chicago, IL, USA) in B-mode, with a linear array ultrasonic transducer (10 MHz). The materials were fixed at 3 cm underwater and presented in a coronal plane. The most suitable glass beads were selected for further concentration tests (Tan et al., 2021).
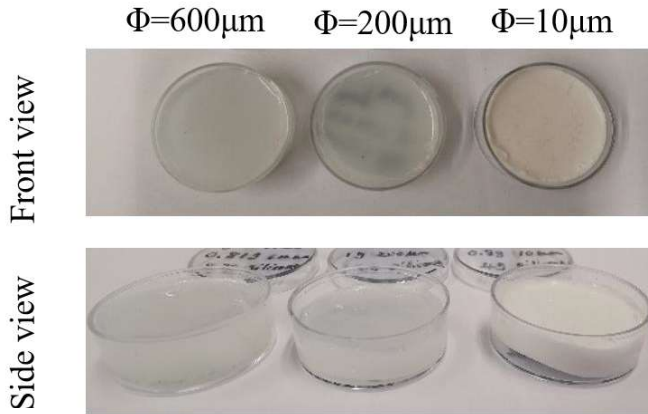
Figure 18. The setup for the influences of glass beads with different diameters (φ=10 µm, 200 µm, and 600 µm) on the echogenicity (from own recording).

Different concentrations of glass beads in the mixtures (weight ratio= 2.5%, 5%, and 20%) was set up for the proportion test. The fabrication method followed the same method of ECOFLEX preparation in section 2.3.3. The fabricated samples were imaged by ultrasound at the identical conditions mentioned in section 2.3.3. Subsequently, according to the imaging result, the most suitable concentration was selected for the molding process of the whole phantom. Figure 19 shows the samples for the concentration test.

Figure 19. The setup for the influences of glass beads with different proportions (φ=10 μm, weight ratio: 2.5%, 5%, and 20%) on the echogenicity (from own recording).

2.3.4. The fabrication process of the whole liver phantom

The fabrication of the liver mechanical simulator is depicted in Figure 20. The liver phantom's inner mold with a bounding box size (~178×120×110 mm^3) was printed on a 3D commercial printer (Object 260 Connex, Stratasys) using a rubber-like photopolymer Tangoblack+ material (Stratasys, Israel) (Fig. 20a). And the outer configuration of the liver model with a bounding box size (~167 × 127 × 124 mm^3) was printed on a 3D commercial printer (Stratasys Fortus 450mc, Stratasys) using ABS material (Fig. 20b). The negative outer molds were created using silicones polymers (Mold Star™, Smooth-On, PA, USA) based on the printed ABS liver. The Mold star was stirred by a glass rod, with a 1:1 by volume ratio of Part A: Part B, and cured for 4 hrs at 64 °C, finally, the printed ABS liver model was removed mechanically. After that, the inner mold was connected to the outer mold by repositioning the extrahepatic ducts in the outer mold (Fig. 20d). As a result, the inner mold was assigned to the proper position corresponding to the outer molds for injection molding. Four positioning pins (3 mm × 3 mm ×10 mm) was used to secure the outer molds. A silicone polymer (Ecoflex 0020, Smooth-On, PA, USA), as well as glass beads, was thoroughly mixed mechanically and

poured into the assembled mold. The diameter of the glass beads and the concentration were confirmed by preliminary experiments (wt% =1%, φ=10μm), see the details in the result section 2.3.3. The polymer material mixture was cured in an oven at a temperature of 65 °C for 4 hours. The inner mold was mechanically removed. It is extractable due to the high degree of elasticity of the inner mold material (Fig. 20e). Extrahepatic biliary tracts were created using the tip-coating technique. The mold for the extrahepatic biliary tract was immersed in another silicone rubber material (Dragon Skin™, Smooth-On) containing the same concentration of glass beads and then gradually removed. After curing overnight at room temperature, a thin layer of silicone polymers was formed. Finally, a liver mechanical simulator with biliary tract was created using silicone adhesive and the extrahepatic biliary duct (Fig. 20f) (Tan et al., 2021).
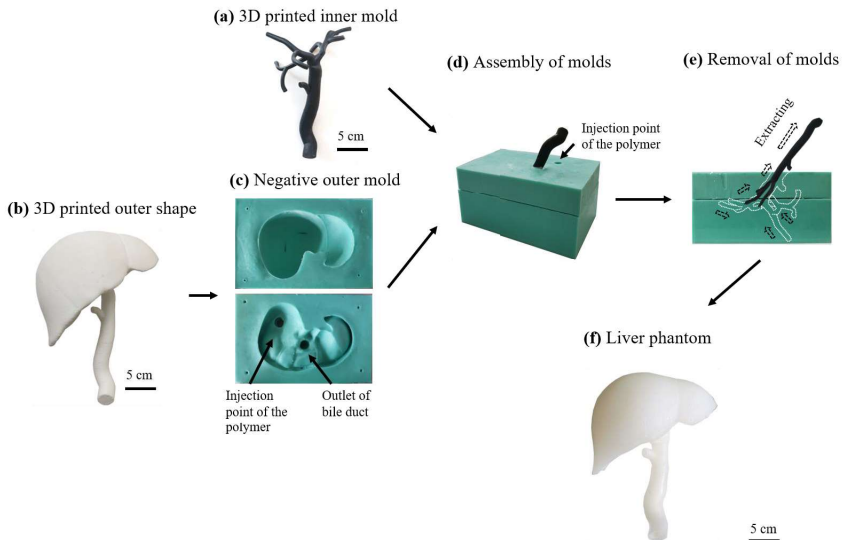
Figure 20. Workflow of fabricating the liver mechanical simulator. (a) the 3D printing of the inner mold with a soft material; (b) the 3D printing of the outer shape of the liver with a rigid material; (c) the negative outer mold; (d) the assembly of inner and outer molds; (e) the demolding process; (f) the fabricated liver phantom. (Tan et al., 2021)

2.4. The validation of the liver phantom

2.4.1. Validation of the liver phantom using radiographic imaging

As illustrated in Fig. 21a, the liver mechanical simulator was examined using a CT scanner (Somatom Force, Siemens, Germany). The data were collected in the axial plane, the matrix size was set as 512 × 512, the field of view was set as 370 mm × 370 mm, and the thickness of the slice was set as 1 mm. The obtained data was saved as IMA file, and were then reconstructed in a 3D medical imaging software (InVesalius v3.1.1, Renato Archer Information Technology Center, Brazil). The 3D structures of the biliary tract and the outer shape of the liver were rebuilt independently. The biliary tract was reconstructed using a threshold of -1024 to -678 Hounsfield units (HU), and the liver using a threshold of -478 to 1144 HU. The quantitative analysis of the fabrication accuracy was processed using mesh editing software (CloudCompare v2.11) by comparing the differences between the 3D reconstructed models and the 3D digital models of the liver. Two identical meshes in the STL files were manually aligned. Then, the cloud/cloud distances between the fabricated and designed models were calculated, as well as the point-to-point distances. Finally, the pseudocolor images were displayed to demonstrate the spatial inaccuracies of the two models. To analyze the difference, the root mean square error (RMSE) of the distance between the fabricated liver mechanical simulator and the designed liver model was calculated. The RMSE is the square root of the distance between the designed and fabricated models (Tan et al., 2021).

Figure 21. The phantom in a CT scanner (from own recording).

2.4.2. Validation of the liver mechanical simulator using endoscopy

The biliary duct was inspected by a flexible endoscope to validate the fidelity of the liver phantom. To visualize the biliary system's "mucosal surface" in the liver mechanical phantom, a thin 16 French endoscope (Slim video gastroscope, Karl Storz SE & Co. KG, Germany) was used. The scope was connected to a light source (XENON 100 SCB, Karl Storz, Germany) and a camera control unit (Image1 S X-link, Karl Storz, Germany), and real-time visualization was provided by a high-definition monitor (9619 NB, Karl Storz) (Tan et al., 2021).

2.4.3. Validation of the liver mechanical simulator using digital type-B ultrasonic imaging

To validate the ultrasonic imaging of the liver phantom, a medical ultrasound imaging platform (LOGIO P6, GE Healthcare, Chicago, IL, USA) was used. A linear array ultrasonic transducer operating in B mode (10 MHz) was used. The liver phantom was submerged approximately 2 cm beneath the surface of the

water and displayed in the coronal plane. The biliary system's anatomical structures were visualized sequentially, including the segmental bile ducts, left hepatic duct (LHD), right hepatic duct (RHD), common hepatic duct (CHD), common bile duct (CBD), and cystic duct (CD) (Tan et al., 2021).

2.5. The simulation of transhepatic puncture procedures and the needle tracking system on the liver phantom

2.5.1. The simulation of transhepatic puncture procedures

As shows in Figure 22, the target bile duct was visualized with the digital type-B ultrasonic imaging system. The parameters of the ultrasound system were set as the same as the parameters mentioned above. Transhepatic puncture procedures were performed using a puncture needle with 20-Gauge (Becton Dickinson S.A., Madrid, Spain). The interrupted needle insertion technique was utilized for puncturing the hepatic parenchyma until the tip of the needle was placed in the target bile duct. The transhepatic puncture procedure was repeatedly performed three times in each bile duct (Tan et al., 2021).
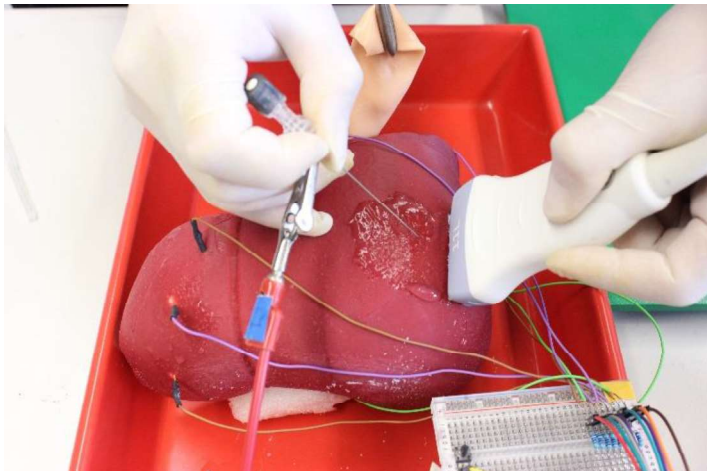
Figure 22. The simulation of transhepatic puncture procedures (from own recording).

2.5.2. The establishment of the needle tracking system and the quantitative

To determine whether the puncture needle was successfully intubated into the target bile duct, a needle tracking system was established. The schematic diagram of the transhepatic needle tracking platform is shown in Figure 23. Eight electrodes (E1–E8), i.e., straight pin headers (RS Components GmbH, Germany), were installed at the respective bile duct tips (B1–B8). A microcontroller (MEGA 2560, Arduino, Italy) was connected to the electrodes and interfaced with a laptop computer. The biliary system was fully filled with 0.9 wt% physiological saline (0.9% NaCl solution), imitating the biliary liquid. The Saline solution functions as an electric conductor in the circuit system. After performing the transhepatic puncture procedure successfully, the needle contacts the physiological saline solution, forming an enclosed circuit system. Different amounts (distances) of saline water between the electrodes and the needles could act as unique resistors (from R1 to R8). Two electrodes, i.e., the transhepatic needle and the reference resistors (R0, 470 Ω), were empowered with a square pulse, with an amplitude of 5.0 V and a period of 0.3 ms. The voltages across the reference resistors (R0) from the eight channels were monitored in order to determine the corresponding resistors for the buffered saline (R1 to R8). The transhepatic puncture needle position was determined by identifying the lowest resistance value, i.e., the shortest conductive path in buffered saline solution. Through analyzing the resistances between the needle and a counter electrode, the accuracy of the needle tracking system was also explored, the schematic diagram of the set-up shows in Figure 24 (Tan et al., 2021).
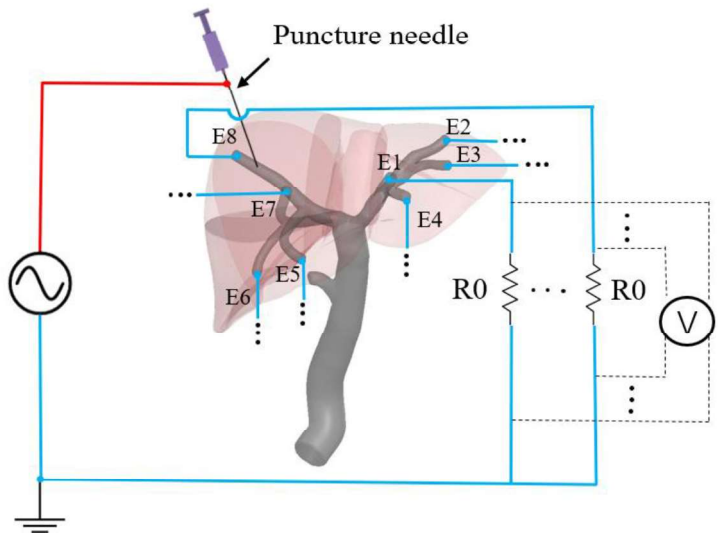
Figure 23. The schematic diagram of the electric sensing system. Eight electrodes (E1-E8) were placed at the tip of each segmental biliary tract, which filled with physiological saline water and the resistance is measured respectively. (Tan et al., 2021)
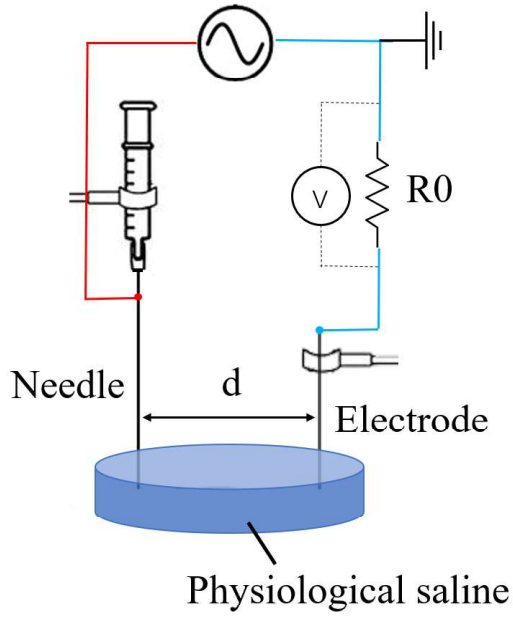
Figure 24. The schematic diagram of the set-up to calibrate the accuracy of the electric sensing system. (Tan et al., 2021)

3. Results

3.1. The feasibility of the fabrication approach and the selections of materials

3.1.1. The feasibility of fabrication approach

To test the possibility of the fabrication approach, a small sample with a bifurcation structure was 3D printed on a commercial 3D printer, using a rubber-like photopolymer material (Tangoblack+). The small samples, served as an inner mold, were then immersed in a cube box filled with silicone-based polymers (ECOFLEX 0020) for molding. After the silicone-based polymers were cured in an oven at 65 °C overnight, the small sample was carefully removed from the silicone-based polymers by extracting force. The result shows that the small sample can be extracted successfully from the silicone-based polymer, which suggested that the fabrication approach described herein is feasible. This method successfully builds a complex hollow structure by the design of the flexible inner mold, which can easily demold from an outer mold without destroying the inner mold (Tan et al., 2021).

The surface of the small sample was carefully inspected to see the potential damages of the fabrication process on the inner mold. Meanwhile, the silicone-based polymer was cut in a coronal plane to expose the surface of the hollow structure, subsequently to explore the potential damages of the fabrication process on the fabricated model. The results reveal that there is no crack in both the inner mold and the fabricated model, which means the fabrication approach herein does not destroy the fabricated model and the inner mold. Therefore, the fabrication method can serve as an ideal approach for the fabrication of a liver phantom with complex hollow structures, e.g., biliary system.

3.1.2. The selections of materials for inner mold (3D printing bile duct)

To find out the best 3D printing materials for the inner mold, different photopolymeric materials with different mechanical properties were selected. In

total, four types of photopolymer materials were included in the material test, i.e., Tangoblack+, FLEX9060-DM, FLEX9095-DM, and RGD8730-DM. Eight samples with two sizes (φ=3-4 mm and φ=1-2 mm) were printed using the above 3D printing materials. Eight samples were then respectively immersed and fixed in eight cube boxes filled with silicone-based polymer (ECOFLEX 0020). After the polymer was cured, eight samples were carefully and mechanically removed. The results show that two samples printed by RGD8730-DM were broken in the bifurcation during the demolding process. However, the other six samples were all successfully removed by the extracting force. Therefore, 3 types of materials, including Tangoblack+, FLEX9060-DM, FLEX9095-DM, are suitable for the fabrication process of the inner molds.

A slim 16 French gastroscope (Slim video gastroscope) was applied for the endoscopy check of six small samples. The inner surfaces of six samples were clearly visualized by the endoscope, see examples in Figure 25. The results show that there is no damage or crack in the inner surface of the six remained samples, which indicates that these materials do not lead to any damages to the liver model (Tan et al., 2021).
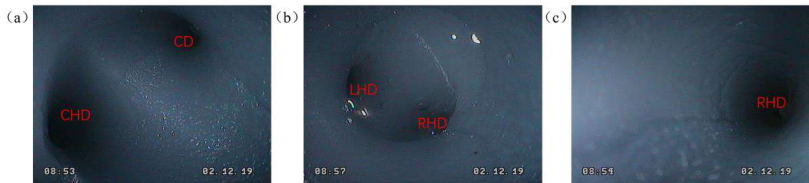
Figure 25. Endoscopic imaging for the small samples of the inner mold. (a) the scope was placed at the common bile duct; (b) the scope was placed at the common hepatic duct; (c) the scope was placed at the right hepatic duct. CHD, common hepatic duct; CD, cystic duct; LHD, left hepatic duct; CHD, common hepatic duct; RHD, right hepatic duct (from own recording).

A digital type-B ultrasonic imaging machine was applied for the ultrasound check of six small samples (simplified bile duct model). Some of the important anatomic structures were inspected in each sample, including common bile duct, cystic duct, right hepatic duct, and left hepatic duct. An example of the small samples was shown in Figure 26. The results show that six remained samples were all clearly visible in the ultrasound imaging system.
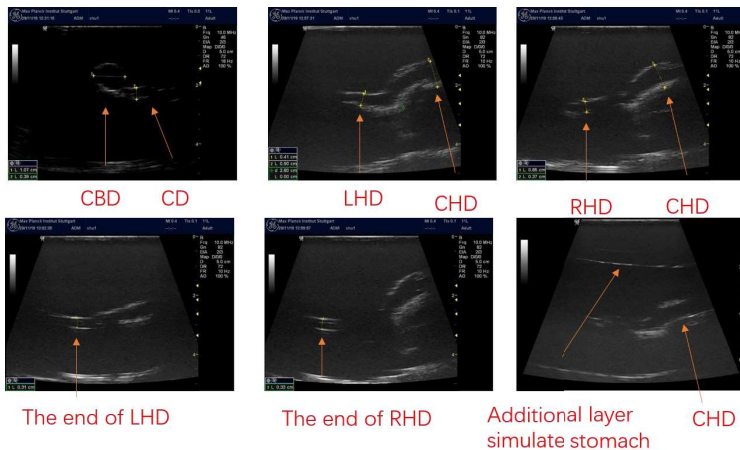
Figure 26. Ultrasound imaging for the small samples of the inner mold. CBD, common bile duct; CD, cystic duct; LHD, left hepatic duct; CHD, common hepatic duct; RHD, right hepatic duct (from own recording).

3.1.3. The selections of materials for the liver parenchyma

According to previous experience, the silicone polymer (ECOFLEX 0020, Smooth-On, PA, USA) is an ideal material that has similar mechanical properties to that of human organ tissues. However, ECOFLEX 0020 is anechoic when undergone ultrasound examination, which is contradicting to the acoustic properties of human liver tissue. Generally speaking, the echogenicity of the hepatic parenchyma is an equal echo. Therefore, to resemble a realistic echogenicity of the liver tissue, the following experiments were performed to explore the most suitable mixtures that resemble the ultrasonic signal of real human liver tissue.

Due to the refraction and scattering effects of glass beads, they can be added into the silicone polymer to increase the amount of echo return to the ultrasound device so that the iso-echogenic signal can be simulated. Therefore, different diameters of glass beads with different weight ratios were mixed with the silicone-based polymers to investigate the best material and proportion of glass beads in the silicone-based polymers.

Figure 27 shows the ultrasound result of the selection of glass beads with different diameters. Three kinds of glass beads (φ= 600 μm, 200 μm, and 10 μm) were added into the silicon-based polymers (ECOFLEX 0020). After curing in the oven at 65 °C overnight, the samples were inspected by a digital type-B ultrasonic imaging machine. The results show that all three samples that mixed with different glass beads exhibit uniform echo signal, which demonstrated that the mixture of glass bead provides a method to produce echogenicity in silicone-based polymers. However, the echo signals in Figure 18a and 18b mainly presents in the bottom of the samples, while the top of the samples remains anechoic. The phenomenon occurs basically because the density of these glass beads (φ= 600 μm, 200 μm) is higher than that of silicone-based polymer and subsequently the glass beads agglomerated to the bottom. Although the glass beads were thoroughly mixed with polymers, they sank to the bottom during the curing time. On the contrary, the glass beads in Figure 18c are equally distributed. This is because the density of the glass beads (φ= 10 μm, ρ =1.1 g/ml) is similar to that of silicone-based polymers (ρ =1.07 g/ml). Therefore, the glass beads can almost be equally distributed in the silicon-based polymers during the curing time, accordingly, the echo signal produced by the glass beads is equally distributed on the top. The result of the material test for the selection of glass beads displayed that the glass beads with a diameter around 10 μm are the most suitable supplement in the silicone-based polymer to resemble the echogenicity properties of human liver tissue.
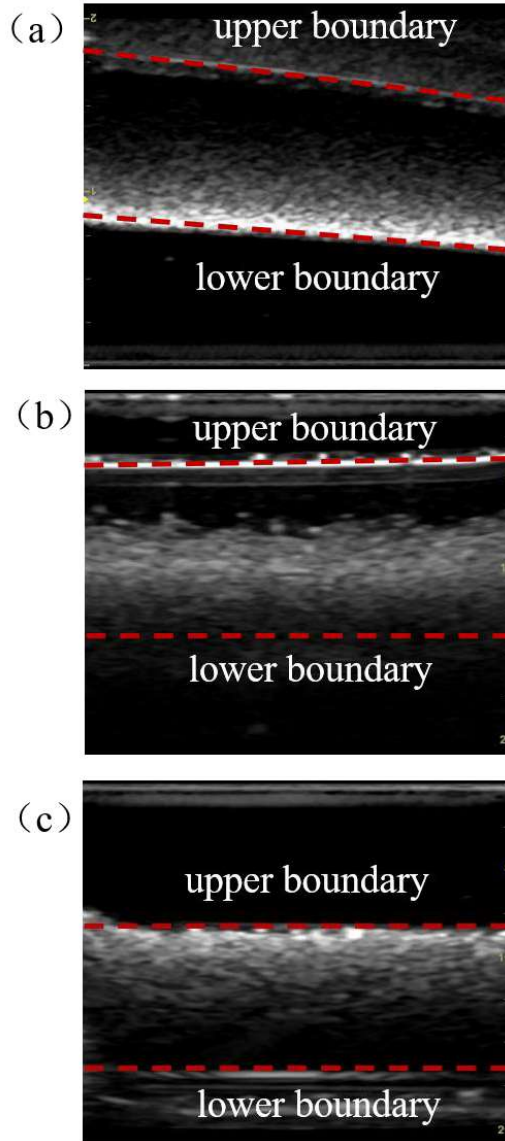
Figure 27. Ultrasound image of the silicon-based polymer samples with different glass beads. (a) Glass beads with a diameter of around 600 μm were added to the polymers; (b) Glass beads with a diameter around of 200 μm were added to the polymers; (c) Glass beads with a diameter of around 10 μm were added to the polymers (from own recording).

To find out the most suitable concentration of the glass beads in the silicone-based polymers, three small samples were made in Petri dishes as molds with a diameter of 3.5 cm. The glass beads with different weights (0.1 g, 0.2 g, 0.8 g, $\varphi=$ 10 μm) were added to 4 g mixtures of silicone-based polymers (ECOFLEX 0020). Therefore, the weight ratios of glass beads in these three samples are 2.5%, 5%, and 20%, respectively. Three samples were then inspected by a digital type-B ultrasonic imaging machine. The appearances of these samples are presented in Figure 19. As shown in Figure 28, all three samples clearly show echo signals during the ultrasound examinations. Furthermore, with more proportion of glass beads in the samples, the echo signals are stronger. It seems that the signal in Figure 19c presents a similar echogenicity to that of real human liver tissue (Figure 8). However, with detailed observation in those images, unequal distributions of ultrasound signals can be detected in Figures 19a, 19b, and 19c. Paradoxically, the distribution of glass beads is homogeneous because the density of glass beads is almost equal to that of silicone-based polymers. Therefore, the reason that results in unequal distribution of ultrasound signals is something else other than the physical distribution of glass beads. After the literature review, we considered that the inhomogeneous ultrasound signals come from the high ultrasonic attenuation of the silicone and glass beads. The speed of silicone-based polymer is considerably lower than that of a real human liver. As a result, the silicone-based polymer has a disadvantage in ultrasound-based imaging. However, the silicone-based polymers (ECOFLEX 0020) were selected mainly because of their durability. This property is essential for the procedure of needle puncture. To reduce the acoustic attenuation, a less proportion of glass beads are supposed to add in the preparation of molding material.

Finally, silicone-based polymers with 1 wt% glass beads ($\varphi=$ 10 μm) were considered as the suitable mixtures as the molding material.
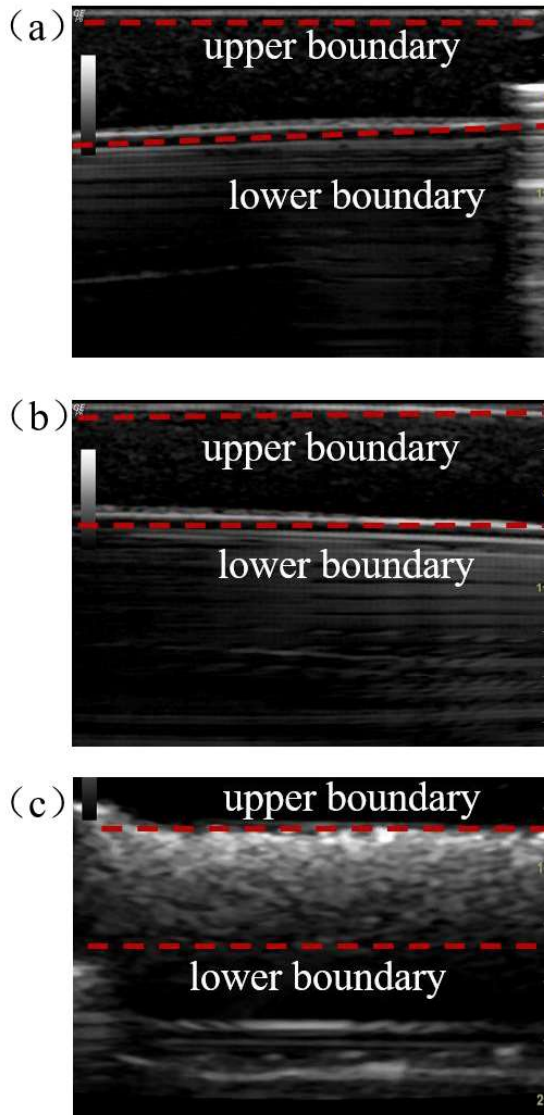
Figure 28. Ultrasound image of the silicone-based polymer samples with different proportions of glass beads. (a) 2.5 wt% Glass beads were added to the polymers; (b) 5 wt% glass beads were added to the polymers; (c) 20 wt% glass beads were added to the polymers (from own recording).

3.2. The fabrication results of the liver mechanical simulator

With the fast development of medical interventional procedures, the potential medical imaging methods for the assistance of interventional procedures have become increasingly versatile. Currently, the most popular interventional imaging are radiophotography, sonography, and endoscopic imaging. To adopt different interventional imaging methods, two different liver phantoms were fabricated.

3.2.1. The fabrication of the liver phantom for the simulation of transhepatic puncture procedure

Most transhepatic interventional procedures are based on the transhepatic puncture procedure, e.g., percutaneous transhepatic cholangiobiopsy, percutaneous transhepatic cholangiography (PTC), percutaneous transhepatic cholangiodrainage (PTCD), and so on. There are no biliary mucosal details involved during the whole interventional procedure. Therefore, the biliary mucosa was not fabricated in the liver phantom for the *transhepatic puncture procedure*. The details of fabrication processing for the liver phantom were illustrated in Figure 11 (Tan et al., 2021).

A soft translucent liver phantom with a hollow biliary system was fabricated. The appearance of the liver phantom from different angles is shown in Figure 29. The results of the liver phantom show that most anatomic landmarks are accurately depicted in the liver phantom, such as the gallbladder bed, the porta hepatis, gastric impression, and so on. This indicated that the phantom herein can serve as high-fidelity organ phantom for medical training (Tan et al., 2021).

Front side

Back side

right side

Figure 29. The view of the liver phantom for the transhepatic puncture procedures. The front view, back view, and right view of the liver phantom were exhibited (from own recording).

3.2.2. The fabrication of the liver phantom for the cholangioscopy-based interventional procedures

Some of the hepatic interventional procedures are based on cholangioscopy, for example, percutaneous transhepatic cholangioscopy (PTCs), peroral cholangiography (POC), and peroral transluminal cholangioscopy (PTLC). These interventional procedures were mainly to inspect the inner structure or lesion in the biliary system. Hence, the mucosal surface of bile ducts is of significant importance. To fabricated the mucosa surface of bile ducts, a thin layer of silicone-based polymers was applied to the inner mold by a dip-coating approach. After the manufacture of the biliary mucosa, the fabrication procedure followed the protocol described in Figure 20.

As shown in Figure 30, a soft and opaque liver mechanical simulator with a hollow biliary system was fabricated. The inner color, surface, and structure of the bile duct highly resemble to that of real human liver tissue. Similarly, most anatomic landmarks are vividly displayed in the liver phantom, including the gallbladder bed, the porta hepatis, and the gastric impression, and so on. This result suggests that the fabricated liver phantom is highly realistic, which is possible for the simulation of the cholangioscopy-based interventional procedures. Furthermore, the fabrication method herein is reproducible and with high accuracy.

Figure 30. The view of the liver phantom for the endoscopy-based interventional procedures (from own recording).

3.3. The validation of the fabricated liver mechanical simulator

To validate the feasibility of the interventional procedures in the liver phantom, the most common medical imaging methods are used, including CT imaging, sonography, and endoscopy. The liver phantom was inspected by these imaging devices sequentially. The results of each imaging method are shown below.

3.3.1. CT validation of the fabricated liver mechanical simulator

The fabricated liver mechanical simulator was placed in a coronal plane and then checked by a CT scanner. The obtained data was imported and reconstructed in 3D medical imaging software. A quantitative analysis of the accuracy of the fabrication process was performed in a mesh editing software, by comparing the digital fabricated phantom model with the original designed model (Tan et al., 2021).

The quantitative error analysis of the biliary system was performed to determine the consistency of the fabrication process of the biliary tract. As illustrated in

Figure 31, the biliary system has a RMSE of 1.7 mm and a standard deviation (SD) of 0.7 mm. The size of the biliary system (a bounding box) measures approximately 147.3 mm in length, 115.6 mm in width, and 243.2 mm in height. As a result, the mean error of the bile duct model is approximately 1%. Because of the flexibility of the printed inner mold, the largest error of the fabrication process (represented by the red colors in Figure 22) occurs primarily at the tip of the biliary system.
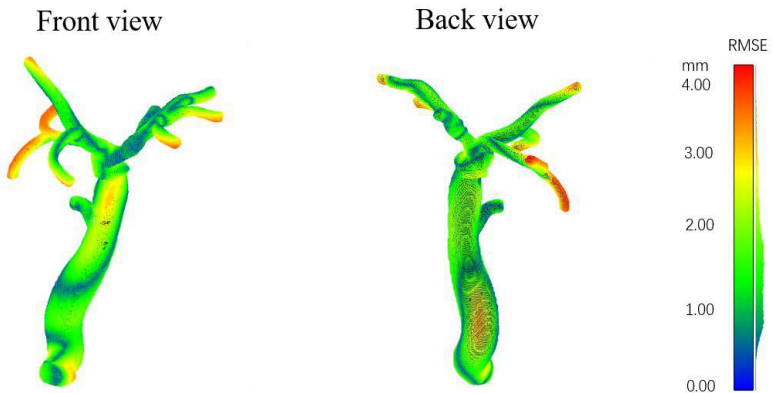
Figure 31. Quantitative error analysis of the bile duct in the liver mechanical simulator compared to the digital model. The surface colors stand for the root mean square error (RMSE). (Tan et al., 2021)

To detect the fabrication process's accuracy of the hepatic parenchyma, the quantitative error analysis of the liver outer shape was performed. As shown in Figure 32, the spatial error associated with the outer shape of the liver phantom is 0.9 mm with an SD of 0.2 mm. Meanwhile, the bounding box of the liver measures approximately 209.4 mm in length, 159.3 mm in width, and 157.6 mm in height. Hence, the mean spatial error of the hepatic parenchyma is less than 0.7 percent. The red mark in Figure 32 that represents the largest error of the liver phantom mainly locates on the visceral surface of the liver (Tan et al., 2021).

The spatial error results of both the biliary system and the hepatic parenchyma imply that the fabrication process precisely resembles the designed model, with

high-fidelity morphological structures in both the biliary system and the hepatic parenchyma. The preciseness of the fabrication procedure, e.g., the mold establishment and the assembly processing, is high. These characteristics of the fabrication process are able to make the liver phantom suitable for the training of interventional procedures (Tan et al., 2021).
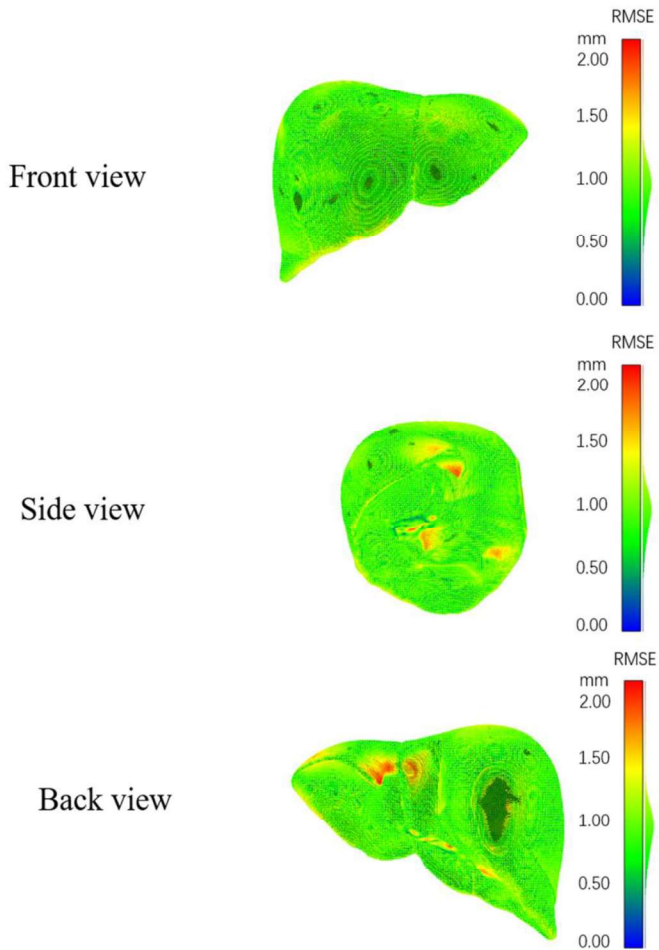

Figure 32. Quantitative error analysis of the liver outer shape in the liver simulator compared to the digital model. The surface colors stand for the root mean square error (RMSE). (Tan et al., 2021)

3.3.2. Endoscopic validation of the mechanical simulator

The opaque liver mechanical simulator with biliary mucosa was assessed using an endoscope, to validate the feasibility of cholangioscopy. As exhibited in Figure 33, the mucosal details of the bile duct in the opaque liver mechanical simulator correctly replicate the typical features of a human biliary system, for instance, the morphological features, surface's color, and texture, and so on. All branches of the bile ducts are able to be intubated with the endoscope. And the inner structures of the biliary system are all clearly visible. The spatial orientation of the endoscope is obtained as in a real human liver (Tan et al., 2021).

Gastrointestinal endoscopists were recruited to perform the endoscopic assessment on the opaque liver mechanical simulator. According to the qualitative assessment of the endoscopists, the tactile feedback of the opaque liver mechanical simulator is almost the same as that of a real human organ during the endoscopic simulation. When the endoscope passes through the bifurcation of the right and left intrahepatic ducts, the feedback becomes even more realistic. This is largely due to the soft silicone polymers used to construct the liver mechanical simulator. The material's elastic modulus is up to 60 kPa (Adams et al., 2017), which falls within the normal range for human liver tissue (0.5-70 kPa) (Żmudzińska et al., 2018). When the scope is performed incorrectly but continuously intubated, a greater resistance can be perceived at the tip of the endoscope. The haptics offer a high-fidelity scenario as if the endoscopists are operating the endoscopy on a real clinical case (Tan et al., 2021).
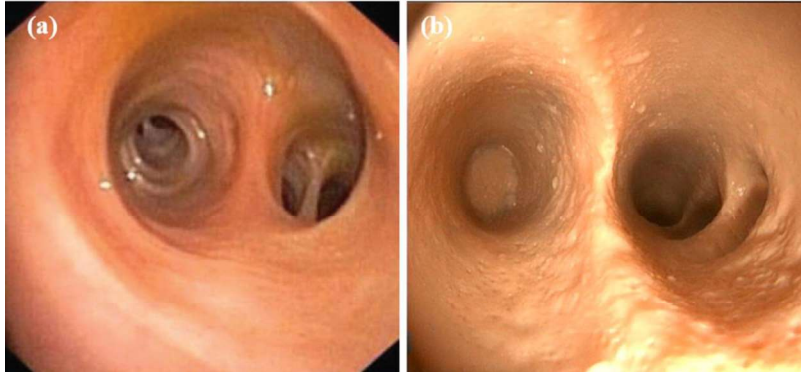
Figure 33. Validation of the liver mechanical simulator using endoscopy. (a) The view of the biliary system in a real human liver. The picture is taken from Ref. (Leung et al., 2011, Parsi, 2011). (b) The view of the liver mechanical simulator. (Tan et al., 2021)

3.3.3. Ultrasound validation of the liver mechanical simulator

An ultrasound examination was used to confirm the ultrasonic imaging in the liver phantom. The ultrasonic results of a real human liver is obtained from a clinical case as a reference (Vardevanyan et al., 2017), which is set as a comparison. As shown in Figure 34, the liver phantom truly replicates the echogenicity of the real human liver compared to the real ultrasound image in Figure 8. For example. the shape of the bile duct and the boundary of the liver were clearly visualized undergoes the ultrasonic examination. Meanwhile, both the intrahepatic and extrahepatic ducts are distinctly identified and traced in the liver mechanical simulator. Figures 25a to 25f show the ultrasonic images of different segments in the biliary system, including medial segmental duct (MSD), right hepatic duct (RHD), left hepatic duct (LHD), common hepatic duct (CHD), cystic duct (CD), and common bile duct (CBD). Other segmental biliary tracts are also able to be observed in the liver phantom. Furthermore, the echo signal from the parenchyma of the liver in the liver phantom exhibits high-fidelity scattering effects as a result of the mixed hollow glass beads in the silicone polymers material. However, the biliary tract, which is located over 4 cm beneath the surface, cannot be visualized clearly; this is primarily due to the silicone material's high acoustic attenuation (Cafarelli et al., 2016). As mentioned above, the silicone-based polymers material ECOFLEX 0020 has a speed of sound (SOS) around 993 ~ 1074 m/s, which is

significantly lower than that of a human liver around 1600 m/s (Cafarelli et al., 2016). However, the fabrication technique described herein is generic and could be applied to other materials, such as composite hydrogels with acoustic properties comparable to those of human organ tissues (Choi et al., 2020, Tan et al., 2021).
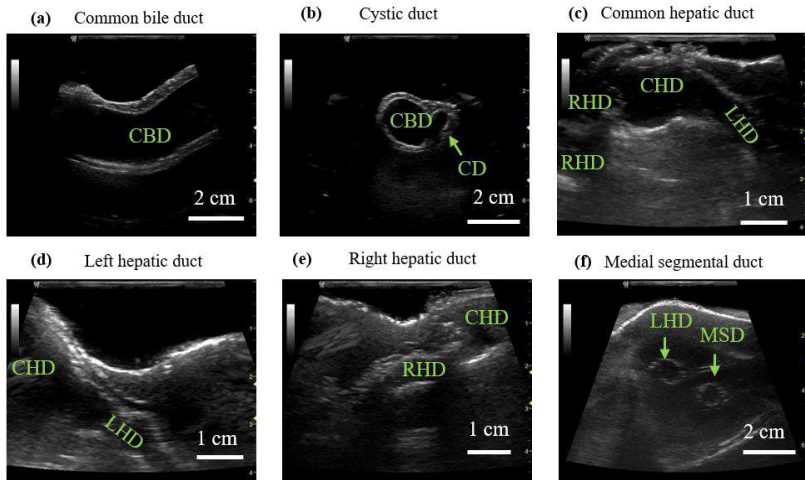
Figure 34. Ultrasonic results of the liver mechanical simulator in different locations (a-f). IHD, intrahepatic duct; CD, cystic duct; CBD, common bile duct; LHD, left hepatic duct; RHD, right hepatic duct; CHD, common hepatic duct; MSD, Medial segmental duct. (Tan et al., 2021)

3.4. Transhepatic puncture procedure simulation on the liver phantom

With the assistance of the digital type-B ultrasonic imaging system, the transhepatic puncture procedure was successfully performed in the liver phantom. Each segmental bile duct is able to be punctured using a 20-Gauge needle. The haptic feedback shows that the resistance of puncturing during the transhepatic puncture procedure similarly resembles that of real human liver tissue. Meanwhile, after several punctures, the liver phantom is still workable. The puncturing path is hard to be observed even if the transhepatic puncture procedures were performed several times. The phenomenon proves that the liver phantom herein is reusable and applicable for the simulation of ultrasound-based transhepatic puncture procedures (Tan et al., 2021).

3.5. The needle tracking system and the quantitative assessment of the transhepatic puncture procedures

A needle tracking system was set up in the liver phantom via an electronic sensing approach. The electrical route in the saline solution is an equivalence of a resistor. By computing the solution resistances, the location of the puncture needle within the biliary tracts can be determined. Then, a calibration experiment was conducted to establish a relationship between the resistance values and the needle-electrode distances (Tan et al., 2021).

To avoid electrolysis, the electrical sensing system used a short pulse with a period of 0.3 ms. During electrical measurements, the saline solution acts primarily as a resistor. To verify the feasibility of the sensing system, a 20-gauge puncture needle was sequentially inserted into the eight segmental bile ducts (B1 to B8) and the resistances of the saline solution (R1 to R8) were measured. The resistance values from R1 to R8 are shown in a log scale in Figure 35. The electrodes with the lowest resistance value are recognized as the puncture site, where the electric path is shortest. Additionally, the smallest resistance value is nearly an order of magnitude smaller than the others (Table 6). For example, when the puncture needle is inserted into B1, the resistance to the nearest electrode R1 is $135 \pm 5\ \Omega$, while the other resistances range from $2341\ \Omega$ to $10050\ \Omega$. Despite the fact that the absolute resistance values of the target resistors may vary due to the needle's location and geometry (such as the diameter and the shape of the tip), the variation in values between the target resistor and other resistors is sufficient to detect the precise location of the puncture needle using a simple threshold approach (Tan et al., 2021).
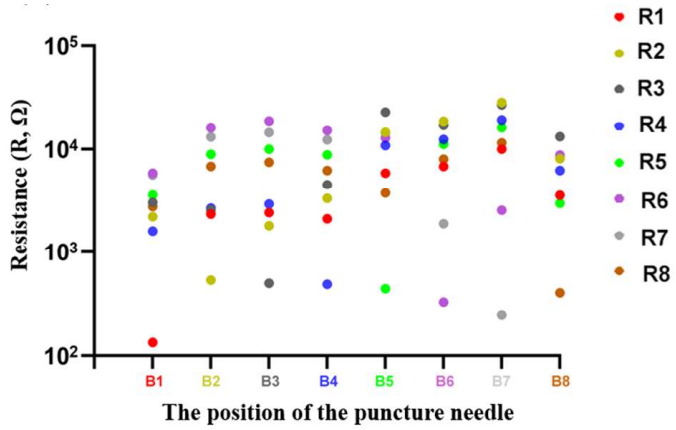
Figure 35. Electrical sensing in the needle tracking system during the transhepatic puncture procedure. (Tan et al., 2021)

Table 6. The recording of resistance changes after the needle was placed in the corresponding bile duct **(from own recording)**.

Resistance (Ω)		Location of the needle							
		B1	B2	B3	B4	B5	B6	B7	B8
R1	Mean	135	2341	2418	2102	5878	6835	10050	3553
	SD	5	20	13	133	126	193	212	27
R2	Mean	2211	533	1799	3321	14563	18496	27939	8118
	SD	11	5	17	237	379	1172	1447	123
R3	Mean	3026	2549	497	4531	22568	17059	26491	13227
	SD	29	31	2	316	1367	898	3158	277
R4	Mean	1601	2670	2918	485	10855	12389	18975	6209
	SD	1	58	17	39	386	10	16	132
R5	Mean	3582	8927	10008	8847	441	11174	16208	2980
	SD	23	138	160	477	26	591	12	17
R6	Mean	5868	16111	18518	15221	12872	326	2554	8796
	SD	48	792	24	938	288	5	38	126
R7	Mean	5644	13108	14493	12356	14333	1885	246	8545
	SD	91	495	355	847	871	31	5	122
R8	Mean	2754	6816	7482	6236	3752	8027	11484	402
	SD	21	74	6	196	67	197	448	4

To assess the spatial accuracy of the electronic sensing approach, a calibration experiment was implemented to explore the correlation between the resistance value and the distance of two electrodes in the saline solution. Figure 36 presents the resistance value of the saline water that adds up linearly with the upturn of the distance ($r^2 = 0.99$) (Tan et al., 2021). Table 7 shows the original recording of the calibration experiment, the resistance of the saline solution (R) is calculated by the following formula.

$$R = \frac{V\text{total}}{\overline{V R0}} * R0 - R0$$

Whereas, Vtotal refers to the electric voltage that powered on the two electrodes (5 V); $\overline{V}$R0 refers to the average of the electric voltages of the resistor R0 which recorded by an oscilloscope. Given the measuring resolution's sensitivity of around 0.1 Ω, the spatial resolution of the reported approach is down to around 0.1 mm.
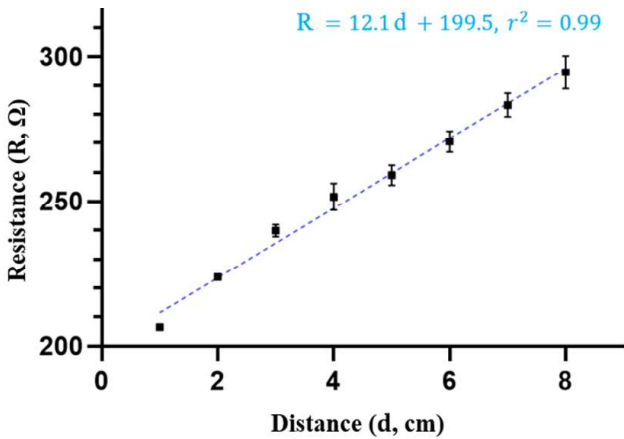
Figure 36. The schematic diagram of the set-up to measure the accuracy of the electrical sensing.

Table 7. The electric results of the calibration experiment for exploring the relationship between distance and electric voltage of R0 in the needle tracking system (from own recording).

Distance (cm)	Electric Voltage (V)	Phase (°)	$V_{R0}1$(V)	$V_{R0}2$ (V)	$V_{R0}3$ (V)	$\bar{V}_{R0}\pm$SD (V)
8	5	10.5	3.06	3.06	3.10	3.07±0.02
7	4.99	10.7	3.11	3.11	3.14	3.12±0.02
6	4.99	11.1	3.16	3.17	3.19	3.17±0.02
5	4.99	10.7	3.21	3.22	3.24	3.22±0.02
4	4.98	10.8	3.24	3.25	3.28	3.26±0.02
3	4.98	10.4	3.30	3.31	3.32	3.31±0.01
2	4.98	10.5	3.38	3.39	3.39	3.39±0.01
1	4.98	10.9	3.47	3.47	3.48	3.47±0.01

Finally, transhepatic puncture procedures on the liver mechanical simulator were performed under the guidance of an ultrasonic imaging device. Randomly, the segmental bile duct (B8) was chosen as a penetration target. A technique known as interrupted needle insertion was applied, which is a common technique that enables the clinical doctor to penetrate easily and reduces the rate of complications. Figure 37 illustrates the needle's ultrasonic image within the segmental bile duct (B8). The record of R8's resistance during the transhepatic puncture procedure is shown in Figure 28b. The period of needle insertion is corresponding to the section from the beginning to Point c. When the puncture needle was inserted into the bile duct, the value of R8 declined promptly. At Section b, a small peak appears with a period of up to 0.6 s. This phenomenon occurs as a result of the needle being withdrawn during the interrupted needle insertion technique. After Point c, when the puncture needle was removed from the bile duct, the value of R8 gradually increased to infinity. Thus, the electrical sensing approach for needle localization demonstrates superior performance in terms of both temporal and spatial resolution.
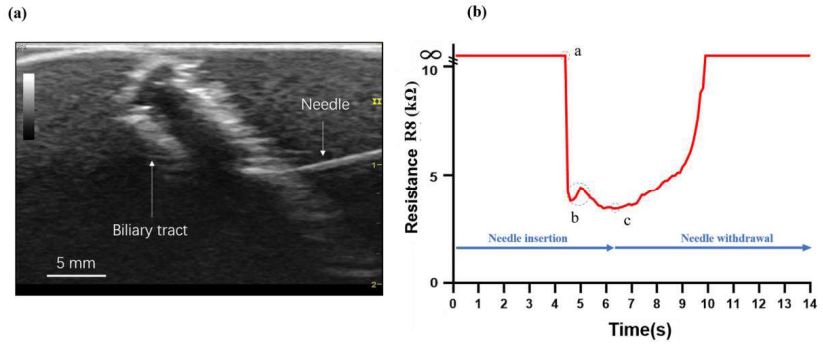
Figure 37. Electrical sensing record during the transhepatic puncture process. (a) The procedure is recorded under the guidance of ultrasound; (b) The resistance change of R8 when the needle was placed in the bile duct (B8). Point a refers to the needle enters the biliary tract; Section b refers to the progressive motion of the puncture needle; Point c refers to start the withdraw of the puncture needle. (Tan et al., 2021)

4. Discussion

In this project, we present a soft liver mechanical phantom that fulfills the characteristics mentioned in the introduction section (1.5). These phantoms utilize soft lifelike material resembling human liver tissues. And several common medical examinations, including CT, ultrasound, and endoscopic imaging, are applied to validate the possibilities of these imaging methods. The phantoms presented herein are able for the wide use of the training of transhepatic interventional procedures, such as EUS-BD, POC, ERCP, and PTCD. Meanwhile, the interventional procedures can be quantitatively evaluated through embedding electrical sensors in the phantom. With the guidance of ultrasound, the precision of the transhepatic needle puncturing is monitored via the real-time electrical resistance measurement. Additionally, distinct segments of the biliary duct can be distinguished. The assessment system enables trainees to engage in interactive interventional training sessions and receive quantitative feedback, which is not possible with existing organ models.

4.1. The fabrication method of the liver phantom

4.1.1. Previous fabrication methods for complex hollow structures

Few studies have reported the fabrication of a complex cavity structure for medical simulators. The complex cavity structures, generally speaking, are hard to build because of the difficulty in the demolding process for the inner mold. Most 3D printers could not print a soft material that resembles the mechanical properties of human tissue (Zheng et al., 2019). Therefore, soft materials molding technologies are needed for the fabrication of cavity structures.

The most common approach to fabricate a cavity structure is designing a dissolvable inner mold. Several 3D printing materials can be used for the dissolvable inner mold. Adams et al reported a novel method of fabricating a human kidney phantom using a 3D wax printing technology (Adams et al., 2017). The collecting system inner mold was printed using wax by a special 3D printer (3Z pro, Solidscape, NH, USA), as shown in Figure 38. The inner mold was then dissolved in the ethanol after the outer shape of the kidney was casted (Adams

et al., 2017).
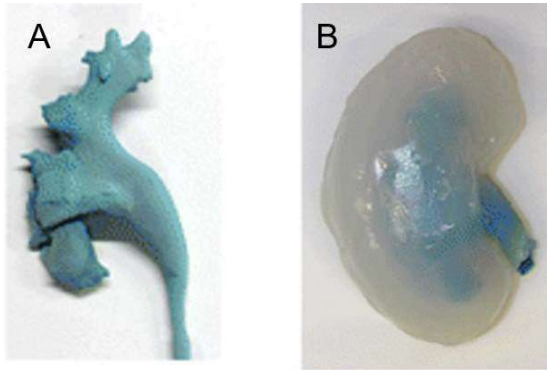
Figure 38. A fabrication method using 3D printed wax to make a complex inner structure. (A) The inner mold is 3D printed in wax. (B) The phantom is demolded from the outer mold, and the inner mold is dissolved in ethanol. (Adams et al., 2017)

Turney et al also reported a water-soluble material to fabricate the cavity structure. In their study, a human collecting model was printed using a 3D printer (Replicator, Makerbot, USA) with polyvinyl alcohol (PVA) material (Turney, 2014). The silicone rubber was solidified in a plastic box that embeds the collecting system inner mold. The PVA inner mold was then removed by immersing it in water. The collecting system model printed by PVA is shown in Figure 39 (Turney, 2014).

In addition, Mashiko et al reported a method of fabricating a hollow and elastic aneurysm model (Mashiko et al., 2015). As shown in Figure 40, a solid aneurysm model was 3D printed using ABS material on a 3D commercial printer (OPT printer, Tokyo, Japan). Subsequently, the ABS material was removed with the toxic solvent xylene after the casting of silicone models (Mashiko et al., 2015).
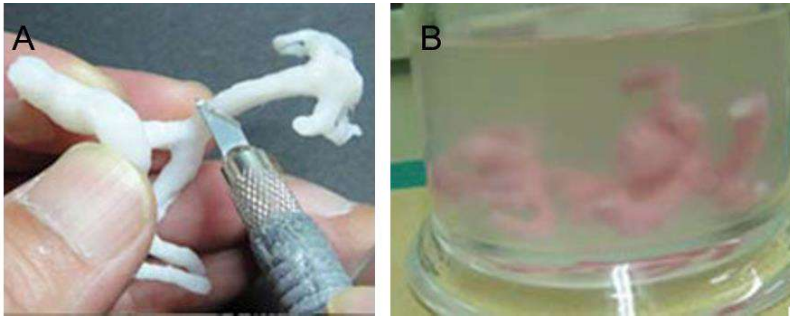
Figure 40. A fabrication method of a hollow elastic model using 3D printed acrylonitrile-butadiene-styrene (ABS) material. (A) the solid ABS model was prepared for the next step; (B) ABS is melted with xylene after silicone solidifies. (Mashiko et al., 2015)

4.1.2. Our fabrication method

In comparison to the previous method, the fabrication used in this study is capable of saving 3D printing material, time, and cost (Adams et al., 2017, Mashiko et al., 2015, Turney, 2014). The inner mold with a complex hollow structure was printed by a flexible 3D printing material (Tangoblack+). The inner mold was then attached to the outer mold, so that silicone polymers can be poured and cured in the assembly of molds. Finally, the inner mold can be extracted from the liver outer shape due to its flexibility. Therefore, a soft liver phantom with the complex biliary system was fabricated to fulfill the requirements of transhepatic interventional simulation. The novel fabrication method herein does not require the sacrificial of the inner mold to fabricate the complex hollow structure. As a result, the inner mold is capable to be reused, which saves time, material, and cost in the 3D printing of the inner mold. Take the kidney phantom by Adams et al as an example, the 3D printing process for the wax inner mold takes almost 1

day (up to 25 hrs). Additionally, the step for dissolving the soluble material is a greatly time-consuming and labor-consuming procedure that is dependent on the solubility of the substance in the solvents. Compared to previous models, the current fabrication method, which utilizes 3D printing and molding technology, enables the creation of an accurate and reproducible soft liver organ model, which can also extend to the pancreas, lung, vasculature, and heart, and so on (Tan et al., 2021).

4.2. Discussion of the materials

4.2.1. The casting material

The casting material is critical for the medical imaging of the organ phantom. Several materials are possible for the fabrication of organ phantoms. But the selections of materials highly depend on the application scenario.

In the ultrasound-based simulation, organ phantoms are usually made from hydrogel materials because of both high cost-efficiency and good performance in connection with echogenicity under ultrasound scanner (D'Souza et al., 2001a, Madsen et al., 1978). For homemade simulators, there are mainly two categories, including the hydrogel categories and plastic categories. For example, the hydrogel family consists of agarose, gelatin, polyvinyl alcohol (PVA-C), and polyacrylamide (PAA), while the plastic category includes polyvinyl chloride (PVC), and so on (Carbone et al., 2012, Casciaro et al., 2009, Madsen et al., 2005). All these mentioned casting material exhibits both advantages and disadvantages. Agarose and gelatin, members of the hydrogel family, are the most widespread materials for resembling soft tissue due to the good acoustic performance, flexible and easy fabrication processes. This kind of material can be fabricated in a fast and harmless way. Yet their characteristics can only be preserved for a limited period because these materials degrade owing to dehydration (Hungr et al., 2012) and microbial invasion (Culjat et al., 2010). Compared to the agarose, the PVA-C can maintain its properties for a longer time – about several months, when stored in a humid and cold environment. Nevertheless, the preparation of 24-hour long freezing cycles is extremely time-

consuming (Chiarelli et al., 2010). The PAA material enables create diverse outlines, however, the surface of the phantom should be smoothed by additional procedures. Zell et al. pointed out that these smoothing procedures can be dangerous during acrylamide polymerization, which could produce neurotoxic and carcinogenic monomers (Zell et al., 2007). The polyacrylamide under certain conditions, such as heat and UV light, can depolymerize to a small quantity of the monomer after manufacturing. The plastic-like material, e.g., PVC, shows significant advantages in the demonstration purpose due to the durability and low cost. But they have limited use for surgical simulation.

The durability of the organ phantom is one of the most important considerations in the fabrication of liver phantom for interventional procedures (Hunt et al., 2013, Madurska et al., 2017). However, the usable life of hydrogel organ simulators is estimated to be 2/3 years and a warranty of 1 year only (Amit et al., 2019, Pacioni et al., 2015). The primary purpose of the liver phantom is supposed to train transhepatic interventional procedures. The phantom made of hydrogel materials is basically disposable after a single use. On the contrary, the organ phantoms made of silicone rubber have an estimated usable life of more than 15 years and come with a warranty of at least 10 years. Therefore, the silicone-based polymers, an organic polymer that consists of a silicone-oxygen chain and organic side-groups I, were chosen as the casting material. Among them, platinum-catalyzed silicones (ECOFLEX 0020) can be vulcanized at room temperature and can resemble similar mechanical properties with a modulus of elasticity of ~60 kPa, which is within the range of human liver tissues. Furthermore, the silicone-based polymers are not prone to fast dehydration, accordingly, the phantom made of silicone does not degrades undergoing ultrasound examinations. The accuracy could decline dramatically when hydrogel materials were exposed to specific high temperature. Silicone-based polymers do not suffer from this effect. The main disadvantage of using silicone-based polymers are the acoustical properties, e.g., sound of speed and attenuation effect, which are not within the range of biological tissues. Consequently, the ultrasonic imaging of the phantom could be difficult owing to the different acoustic properties. With the assistance of augmented reality (AR), the software can compensate the imaging results of the organ phantom (Kunkler, 2006). Also, the results in the literature indicated that acoustic

properties of silicone-based material can be modified using additives (Maggi et al., 2009).

4.2.2. The material for molds

Due to the limitation of the 3D printing materials, some materials that are suitable for the manufacturing of organ phantom, yet, are not available or quite difficult to be produced in 3D printing technology. Take rubber or silicone as an example, although there are several 3D printers that could print those materials, the cost of the special 3D printer and material is extremely high, and the product dimension and resolution are also limited. The 3D printing material problem may be solved in the future. The limitation of direct printing silicone or rubber imposes us to come up with another fabrication method to build a soft and realistic liver phantom. Our fabrication approach, combining the 3D printing technology and soft material molding technology, lower the requirement for the 3D printing material. Therefore, the 3D printing material with high flexibility is applicable in our method.

A 3D printing flexible material refers to the 3D printable material that can be stretched reversibly when it undergoes elastic strain. In our fabrication, the flexibility of the mold material is one of our most considerations. The inner mold can only be removed from the liver outer shape when the material of the inner mold is flexible enough. Several 3D printers with different printing technologies offer flexible materials, the following are the most common,

- FDM (Fused Deposition Modeling): the FDM 3D printing technology builds the productions using a continuous filament of thermoplastic material (Liu et al., 2021, Wissamitanan et al., 2020).
  - ✓ Flexible thermoplastic elastomers (TPE)
  - ✓ Flexible thermoplastic polyurethane (TPU)
  - ✓ Flexible thermoplastic composite pipe (TCP)
- Polyjet: The Polyjet 3D printing technology builds the productions via jetting plenty of photopolymer droplets onto a printing bed and curing them with Ultraviolet (UV) light (Zammit et al., 2020).

✓ Tango resin (photopolymer)

● SLS (Selective Laser Sintering): The SLS 3D printing technology uses laser light to sinters powdery materials, such as nylon and polyamide. The laser can automatically bind the materials together at the points defined by a 3D model (Deng et al., 2018).

✓ Polyether block amide (PEBA)

✓ Polyamide 12 (PA12, slightly flexible)

● CLIP (Continuous Liquid Interface Production): The CLIP 3D printing technology uses the principle of oxygen-inhibited photopolymerization to continuously solidify the photopolymer instead of an iterative layer-by-layer process (Miller et al., 2017).

✓ Elastomeric polyurethane (EPU)

✓ Flexible polyurethane (FPU)

● 3D printing silicone (Abdollahi et al., 2020, Davoodi et al., 2020, Roh et al., 2017)

✓ UV-sensitive silicone (ACEO, Wacker, Munich, Germany)

✓ Catalyst-cross-linker silicone (Fripp Design, Sheffield, UK)

The Polyjet 3D printing technology using Tango resin was selected for the fabrication of the inner mold due to the high resolution and large dimension (Tan et al., 2021).

To compare the flexibility of the printing materials, several mechanical properties were measured, including hardness, and elongation at break. As we mentioned in section 2.3.2, Tangoblack is the softest and the most stretchable materials among the selected materials. The flexibility of Tangoblack is therefore the highest. Considering the large deformation during the demolding process, the most flexible material was identified as a printing material for the fabrication of the liver inner mold.

4.3. The fidelity of the liver phantom

According to the degrees of fidelity, the medical training simulators are usually classified based on their fidelity. However, no broad agreement on "fidelity" was reported in this field. Normally, the fidelity, also known as the concept of "realism", considers the following parameters, including the resemblance of anatomy and difficulties encountered, visual impression, tissue texture, and the ability to acquire the technical skills during the procedure, and so on (Matsumoto et al., 2001, Sarmah et al., 2017). It was reported that a realistic surgical simulator has an essential position in training performance and simulation acceptability (Hamilton et al., 2002).

In this study, the anatomy structure, the imaging results, as well as mechanical properties were exhibited to validate the fidelity of the liver mechanical simulator. The reported liver mechanical simulator exhibits very accurate anatomical structures, particularly in the hollow structures of the biliary system. Additionally, it produces realistic images in a variety of medical imaging modalities, including CT, ultrasound, and endoscopy.

4.3.1. The resemblance of the anatomy structures

Anatomic structures are extremely essential for surgical procedures. The anatomic landmarks can assist physicians in recognizing the functional anatomy of the liver and facilitate segmental dissection during the surgery (Buzink et al., 2010, Muavha et al., 2019, Wang et al., 2018). The locations and shapes of the liver and Glisson's capsule (which ensheathes hepatic artery, portal vein, and bile ducts) are the key points during the surgical or interventional procedures (Hiroyoshi et al., 2019, Rossi et al., 2019).

As shown in section 3.3.1, the described approach accurately replicated the complex 3D shapes of both the liver and biliary system. The shapes of the biliary tract and the corresponding position to the liver also fully resemble that of the designed model. Hence, training different procedures at diverse locations is feasible in our liver phantom, which could greatly improve the efficiency of deliberate practice. Because the strategies and difficulties of transhepatic interventional procedures greatly rely on the position of the lesions, the establishment of liver phantoms with different lesions at different localizations can

71

create an opportunity for simulations of various situations (Tan et al., 2021).

In addition, the liver phantom accurately depicts anatomic landmarks such as the gallbladder bed, the porta hepatis, and the gastric impression. This provides a promising perspective in surgical simulations, which are beyond the transhepatic interventional training (Tan et al., 2021).

4.3.2. The resemblance of the imaging results

As the results are shown in section 3.4, the fabricated liver mechanical simulator also produces realistic imaging results for routine clinical examinations, including CT scan, ultrasound, and endoscopy, allowing for the training of advanced endoscopic procedures (Tan et al., 2021).

The imaging result of the endoscopic validation was reported in Section 3.3.2. The mucosal detail of the bile duct, as well as the morphological features, highly resemble that of the human biliary system. The liver phantoms are therefore possible to be used to train the cholangioscopic procedures, including direct peroral cholangioscopy (POC), percutaneous transhepatic cholangioscopy, or even cholangioscopy-guided lithotripsy.

The ultrasonic imaging data of the liver phantom were shown in section 3.3.3. All the important biliary structures are able to be exposed undergoing the ultrasound examinations, including intrahepatic bile duct and extrahepatic duct, which provides a theoretical basis for the training of ultrasound-based interventional procedures. Although the ultrasonic images' quality is not so high compared to human liver tissue, the biliary ducts are still distinguishable, which could localize the biliary tract and track the direction of the needle.

The CT scan provides high-resolution data to visualize the biliary system and liver parenchyma. The signal of the hollow biliary tract undergoing CT scanning obviously differentiates that of liver parenchyma. This provides the possibilities for CT-guided interventional procedures. Although the hepatic vascular system, such as portal vein and hepatic artery, was not taken into account, the fabrication herein is also possible to be extended to the vascular system. Furthermore, additional lesions composed of different materials can also be embedded in the

liver phantom to replicate diseased cases, such as carcinoma, hemangiomas, and cysts (Tan et al., 2021).

Hence, the liver phantom has already fulfilled the requirements for the training transhepatic interventional procedures. Additional research will be conducted to determine the value of advanced interventional training for surgeons.

4.4. The performance assessment for the simulation of transhepatic puncture procedures

4.4.1. The importance of performance assessment in medical training

Simulation-based medical training is critical for teaching surgical residents how to acquire medical skills without risking patients' lives. It is still a controversial question how to assess surgical performance. Conventionally, surgical skills are evaluated through an examination of the logbook and professional feedback following a period of service. It has been reported that a logbook is not a reliable indicator of expertise (Shah et al., 2001). The reason for this is that the parameters include the number of procedures and supervision code, rather than individual procedure performance scores. Thus, logbooks are deficient in terms of content validity (Cuschieri et al., 2001). Professional feedback evaluates the performances of the trainee by a professional supervisor, which is widely used in medical assessment. Yet the professional assessment is largely subjective and influenced by several factors, e.g., the basic condition of patients, operating theatre's environment, and hospital condition.

Compared to the traditional training approaches – "see one, do one, and teach one", the simulation-based training provides a practical way to achieve the competency credentialing and training assessments (Hohmann et al., 2019, Lal et al., 2020, Sachdeva, 2011). Embedded sensors in the simulators are able to monitor different parameters that are associated with the surgical performance. These parameters enable supervisors to observe objective and reliable factors that cannot be easily recorded (Shah et al., 2001, Shaharan et al., 2014).

4.4.2. The current metrics for the evaluation system

The assessment systems for surgical performance mainly exists in virtual simulators and mechanical simulators. The assessment system has begun to been accepted and applied in simulators, especially in virtual reality simulators. The uttermost advantages of computer-based training are that they can gather a set of quantitative measurements on which training performances and competency level can be objectively assessed. Here, the most frequently used metrics that can evaluate the performance of surgical procedures are summarized below (Oropesa et al. 2011, 2013; Cotin et al. 2002; Escamirosa et al. 2015).

- Velocity-related factors:
    - idle time to indicate inactive period
    - maximum velocity
    - average velocity

- Distance-related factors:
    - angular path
    - depth
    - orientation

- Volume-related factors:
    - energy of volume
    - economy of volume

- Acceleration-related factors:
    - motion smoothness
    - average acceleration

- Force-related factors:
    - average force
    - average torque

- maximum force

- maximum torque

● Area-related factors:

- angular area

- energy of area

- economy of area

● Error-related factors:

- accuracy

- the number of errors

● Collision-related factors:

- the number of collisions

- tissue damage

● Other factors:

- bimanual dexterity

- economy of diathermy

Although there are plenty of metrics for the surgical assessments, the most important metrics depend on which procedure physicians want to be assessed. Take the transhepatic puncture procedures as an example, the metrics that physicians concern most are whether the needle is placed in the right structures, such as bile ducts, and which bile duct is punctured. These parameters directly influence the outcomes of the patients. Therefore, a sensing system aimed at detecting these metrics was developed.

4.4.3. The sensing system in the liver phantom

A unique sensing system was built to evaluate the performance of the transhepatic puncture procedure. The needle tracking system is able to quantitatively assess the performance of the puncture procedure, specifically the puncture location's accuracy. It provides trainees and supervisors with real-time

feedback, measuring several parameters that are difficult to be acquired in real surgeries and organs (Tan et al., 2021).

4.4.3.1. *The assessment of the success rate and the location for needle puncture*

The success of the transhepatic puncture procedure was assessed as the needle puncturing into the biliary system. The localization of the puncture needle, e.g., the segmental ducts, was also evaluated via the sensing system (Tan et al., 2021).

The success and localization of the puncture needle are critical parameters because they are directly related to the success and safety of interventional procedures (Tan et al., 2021). The needle tracking system described in this study elaborately uses an electrical sensing approach to obtain a set of electronic signals to analyze the detailed information regarding the process of puncture. The success of the needle puncturing onto the biliary tract can be estimated by the connection of the electric circuit via the physiological saline. And the localization of the needle could also be tracked through the quantitative measurement of the resistance of the corresponding physiological saline. The calibration experiments show that a considerably high localization accuracy of 0.1 mm.

The electrical sensing approach depicted herein is general and reliable to localize an instrument in the liver phantom for transhepatic minimally-invasive procedures. The electrolysis of water molecules disturbs the sensing under direct current (DC) power. By changing the measurement scheme to alternating current (AC) or short DC pulses, the electrical measurements were reproducible and reliable.

4.4.3.2. *The assessment of the puncturing details during the transhepatic puncture procedures*

As mentioned in section 3.5, the liver system was punctured via a transhepatic puncture procedure. The resistance of R8 was measured and graphed during the B8 puncturing procedure. The resistance curve in Figure 28b depicts the physician's detailed maneuver for an interrupted insertion technique. This is a common technique for puncturing, that utilizes a needle with a higher maximum

insertion force and controllable movement (Tan et al., 2021). It can facilitate puncturing and prevents complications (Forte et al., 2016). After proper needle insertion into the biliary tract, the tiny peak at Section b clearly reveals the needle withdraw, which is consistent with the ultrasonography. It demonstrates the presented sensing approach's high spatial and temporal resolution.

Theoretically, the speed of the puncturing procedure can be calculated through the current change, which is then possible to assess the fine movement of trainees, e.g., the puncturing force. This provides an essential indicator for deliberate training.

Overall, the needle tracking system is capable of assessing puncturing accuracy and providing real-time feedback to trainees, assisting them in learning how to handle sophisticated instruments and honing their surgical skills.

4.5. Perspectives of the liver phantom

Simulation-based training has already proved to be a safe and effective way to acquire competency for surgical training, including interventional procedures (Aggarwal et al., 2011, Fong et al., 2020, Heelan Gladden et al., 2018, Manuel et al., 2021, Ozer et al., 2021, Tedesco et al., 2008). Currently, the interventional procedures regarding liver and bile duct are quite difficult to be performed owing to the technical difficulties and limited clinical cases' volume (Lee et al., 2019, Matteotti, 2019). The liver phantoms with the biliary system that could train those procedures are urgently needed.

The reported fabrication method can build a soft liver phantom with a hollow and complex biliary system, that combines 3D printing technology and soft material molding technology (Tan et al., 2021). Compared to the most common fabrication approaches to fabricate complex hollow structures(Adams et al., 2017, Mashiko et al., 2015, Turney, 2014), the fabrication method herein doesn't need to sacrifice a complex inner mold, so that the inner mold can be repeatedly used. Subsequently, the time, cost, and labor for the manufacturing of the inner molds can be greatly saved, which provides a potential strategy for massive production in the industry.

Furthermore, the capabilities of the liver phantom for multiple modality imaging have tremendously widened the application fields. Although only the transhepatic puncture procedure was simulated in the phantom, the liver phantom has promising perspectives for the interventional simulations if other relevant organs are added. Below are a few possible examples.

4.5.1. The perspectives in therapeutic ERCP

There are several diagnostic ERCP models for the fundamental technical training in both research studies and markets, including ex vivo ERCP models, virtual ERCP models, and mechanical ERCP models (Bittner et al., 2010, Frimberger et al., 2008, Itoi et al., 2013, James et al., 2016, Leung et al., 2012a, Leung et al., 2007, Leung et al., 2012b, Liao et al., 2013, Lim et al., 2011, Von Delius et al., 2009). However, few therapeutic ERCP models were reported (Committee et al., 2019, Jovanovic et al., 2015). As a result of the hollow biliary system, the fabricated liver phantoms are able to train many kinds of therapeutic ERCP procedures, including stone removal, stent placement, balloon dilation, and transluminal biopsy. In addition, the therapeutic procedures can be performed in different segmental ducts, which has to our knowledge not been reported previously.

4.5.2. The perspectives in POC

Few simulators, neither virtual nor mechanical models, are used for the training of direct POC. In 2006, Larghi et al were the first to demonstrate the feasibility of direct POC in three patients using an ultrathin endoscope (Larghi et al., 2006). A few new approaches or accessories have been shown to increase the success rate of POC, for example, the back-through the guide-wire techniques (Moon et al., 2009); the intraductal balloon-guided technique (Moon et al., 2009, Waxman et al., 2010); and the overtube balloon-assisted techniques (Choi et al., 2009, Tedesco et al., 2008), and so on. For the training of POC, five live porcine models were prepared to acquire the skills and experience, which was reported by Lin et al (Lin et al., 2012). The total procedure time has proved to be greatly shortened after the deliberate training. The liver phantom provides detailed mucosal surface

and anatomically accurate shapes of the biliary system, which enable the training of POC, especially in tip control and spatial recognition.

4.5.3. The perspectives in EUS-BD

Currently, most EUS-BD models are established based on animals or animal organs (Dhir et al., 2015, Dietrich et al., 2018, Lee et al., 2014, Minaga et al., 2017). The shortness of these kinds of models cannot be ignored, such as the long duration for preparation, the difficulties in waste disposal, and ethical issues, and so on. Our liver phantom has the capabilities for the training of transhepatic puncture procedure, ultrasonic imaging, and choledochography, which could serve as an ideal mechanical simulator for EUS-BD. Furthermore, the accurate localization of the puncture needle makes it possible to elaborately assess the performance of trainees and give real-time feedbacks, so as to improve their technical skills and competency.

4.5.4. The perspectives in PTCD

PTC or PTCD is a radiological technique that has been popular since 1952 (Carter et al., 1952, Schuberth et al., 2010). It has a special place in the therapy of Cholestatic jaundice, especially in proximal biliary obstruction. However, the training for the procedure is still a problem. Few studies reported a simulator that could be used for the PTCD's training (Fortmeier et al., 2016, Papanikolaou et al., 2014). Animal organ tissue can hardly resemble intrahepatic biliary dilation. Therefore, the manufacturing of a feasible and realistic phantom remains a challenge. Fortmeier et al demonstrated a virtual reality model for the training of PTCD, the haptic interaction, ultrasound imaging, and X-Ray simulation are provided. Undoubtedly, there is still a long way to go due to the limited haptic interaction and the cost problem. Our liver phantoms possess a hollow dilated biliary system, in accordance with the pathological structure. It is a potential cost-effective simulator for the training of PTC/PTCD.

4.6. Conclusion

In summary, transhepatic interventional procedures are technically difficult, and medical training for these procedures is urgently needed. In this study, we have solved several difficulties in the field of organ phantoms for medical training.

The originalities were summarized in the following bullet points.

- We report a cost-efficient and feasible fabrication approach to build an organ phantom with complex inner cavities, which combines 3D printing and molding technologies.

- A soft liver phantom with a hollow biliary system was manufactured. The liver phantom remains high-fidelity and anatomically accurate in both the liver and the corresponding biliary system, including extra- and intrahepatic ducts.

- The validation experiments of the liver phantom in ultrasound, endoscopy, and radiology shows that the liver phantom exhibits realistic imaging results, compared to the imaging data in real human liver.

- The liver phantom is able to be imaged undergoes ultrasound, endoscopy, and CT scanning. The medical training involving these examinations, including X-ray, are possible in the liver phantom.

- The casting material for molding, i.e., ECOFLEX 0020, is durable, analogous mechanical properties to human tissue. Although the acoustic properties are inadequate, the mixing of additives, e.g., glass beads, can improve the similarity in acoustic properties.

- Transhepatic needle puncturing procedure was successfully simulated in the liver phantom (Tan et al., 2021). A quantitative evaluation system was carried out on the phantom to assess the performance of trainees during the training. The position of the puncturing needle and successfully puncturing or not can be precisely assessed in real-time.

The liver phantom shows extraordinary strengths in medical training that involves ultrasound-related procedures, endoscopy-related procedures, and radiology-related procedures, including PTC/PTCD, ERCP, POC, and EUS-BD. It could also find wide applications in medical device testing.

5. <u>Abstract</u>

<u>Introduction:</u> Flexible endoscopy constantly offers innovative diagnostic and therapeutic options for hepatobiliary disorders. These advanced procedures, which are sometimes complex and have relatively high complication rate, require special technical skills, proficient anatomical knowledge and a long learning curve. For the patient-independent training of endoscopic and endosonographic procedures, a soft, true-to-life, and durable liver organ model with detailed morphology should be available. In this thesis, a cost-effective, self-made, and soft liver model with an anatomically correct biliary system is presented.

<u>Method:</u> The 3D printing and soft molding technology were used to produce the complex biliary system embedded in a nearly realistic liver model. The anatomy of the liver model was validated by computed tomography (CT), ultrasound and endoscopy. The interventional transhepatic procedures were initiated based on the liver model. An accurate assessment system for the transhepatic approach was established for the validation of training effects and individual competency.

<u>Results:</u> A realistic liver model was successfully developed and manufactured. CT results show that the liver model reflects the detailed anatomy, with a spatial root mean square error (RMSE) of 0.9 ± 0.2 mm and 1.7 ± 0.7 mm for the external shape of the liver and the bile duct, respectively. The endoscopic and ultrasonographic images of the model are similar to that of real human tissue. The transhepatic puncture of bile ducts was successfully performed in the model and the quantitative localization of the transhepatic needle was accurately conducted by an electronic sensing system in real-time.

<u>Conclusion:</u> The presented artificial liver model for endoscopic and endosonographic training is close to a normal liver. Moreover, it is cheap, reliable and easy to reproduce. The transhepatic puncture procedure can be simulated in the liver model. The electronic sensor module offers an opportunity to objectively monitor the success of the training. The investigations of the liver model in training other advanced interventions are warranted in the future studies, such as Endoscopic Retrograde Cholangiopancreatography (ERCP), percutaneous transhepatic cholangiography or choliangiographic drainage (PTC/PTCD),

percutaneous choledochofiberoscopy (POC), endoscopic ultrasound guided biliary Drainage (EUS-BD).

6. <u>Zusammenfassung</u>

<u>Einleitung:</u> Die flexible Endoskopie bietet eine ständig wachsende Zahl innovativer diagnostischer und therapeutischer Möglichkeiten bei hepatobiliären Erkrankungen. Diese fortschrittlichen Verfahren, die mitunter komplex und gar nicht so selten mit relevanten Komplikationen verbunden sind, erfordern spezielle technische Fertigkeiten, ein profundes anatomisches Wissen und eine lange Lernkurve, die praktisch trainiert werden muss. Für ein patientenunabhängiges Training endoskopischer und endosonographischer Eingriffe sollte ein weiches, naturgetreues und langlebiges Leberorganmodell mit detaillierter Morphologie zur Verfügung stehen. In dieser Arbeit wird ein praktikables und kostengünstiges selbst hergestelltes weiches Lebermodell mit anatomisch korrektem Gallensystem vorgestellt.

<u>Methode:</u> Mit Hilfe von 3D-Druck- und Weichstoffformungstechnologien wurde ein nahezu realistisches Lebermodell mit einem komplexen, hohlen Gallensystem hergestellt. Die Anatomie des Lebermodells wurde mittels Computertomographie (CT), Ultraschall und Endoskopie validiert. Nach Aufbereitung und Auswertung der Bildgebung wurden interventionelle transhepatische Eingriffe eingeleitet. Zur Validierung der Trainingseffekte und der individuellen Kompetenz wurde ein genaues Bewertungssystem für den transhepatischen Zugang etabliert.

<u>Ergebnisse:</u> Ein realistisches Lebermodell wurde erfolgreich entwickelt und hergestellt. Die CT-Ergebnisse zeigen, dass das Lebermodell die detaillierte Anatomie wiedergibt, mit einem räumlichen Root Mean Square Error (RMSE) von 0,9 ± 0,2 mm und 1,7 ± 0,7 mm für die äußere Form bzw. den Gallengang. Das endosonographische Bild des Modells ist realistisch und die Dimension der Gallengänge ist konsistent. Die transhepatische Punktion der Gallengänge war durchführbar und ein elektronisches Abtastsystem zur quantitativen Lokalisierung der transhepatischen Nadel in Echtzeit war erfolgreich möglich.

<u>Schlussfolgerung:</u> Das vorgestellte künstliche Lebermodell für das endoskopische und endosonografische Training kommt der Realität einer

normalen Leber sehr nahe, ist kostengünstig, einfach zu reproduzieren und für die Serienproduktion geeignet. Mit dem elektronischen Sensormodul lässt sich der Trainingserfolg objektiv kontrollieren. Neben der transhepatischen Punktion könnten an diesem Modell weitere Eingriffe trainiert werden, wie z. B. endoskpischen retrograden Cholangiopankreatographie (ERCP), perkutane transhepatische Cholangiographie oder choliangiographische Drainage (PTC/PTCD), perkutane Choledochofiberoskopie (POC), endoskopische ultraschallgeführte biliäre Drainage (EUS-BD).

7. References

Aabakken L (2012) Endoscopic retrograde cholangiopancreatography. Gastrointestinal endoscopy 76: 516-520.

Abdel-Misih SR and Bloomston M (2010) Liver anatomy. Surg Clin North Am 90: 643-653.

Abdollahi S, Markvicka EJ, Majidi C and Feinberg AW (2020) 3D Printing Silicone Elastomer for Patient-Specific Wearable Pulse Oximeter. Adv Healthc Mater 9: e1901735.

ACGME ACGME program requirements for graduate medical education in general surgery. www.acgme.org/acgmeweb/Portals/0/PDFs/archive/409_psychosomatic_PRs_RC.pdf (accessed March 09).

Adams F, Qiu T, Mark A, Fritz B, Kramer L, Schlager D, Wetterauer U, Miernik A and Fischer P (2017) Soft 3D-Printed Phantom of the Human Kidney with Collecting System. Annals of biomedical engineering 45: 963-972.

Aggarwal R and Darzi A (2011) Simulation to enhance patient safety: why aren't we there yet? Chest 140: 854-858.

Ahn JY, Lee JS, Lee GH, Lee JW, Na HK, Jung KW, Lee JH, Kim DH, Choi KD, Song HJ, Jung HY and Kim JH (2016) The Efficacy of a Newly Designed, Easy-to-Manufacture Training Simulator for Endoscopic Biopsy of the Stomach. Gut and Liver 10: 764-772.

Akhaddar A (2018) Jacques-Joseph Bonhomme (1708-1793): Forgotten French Neuroanatomist and Surgeon. World Neurosurg 115: 35-40.

Amit C, Muralikumar S, Janaki S, Lakshmipathy M, Therese KL, Umashankar V, Padmanabhan P and Narayanan J (2019) Designing and enhancing the antifungal activity of corneal specific cell penetrating peptide using gelatin hydrogel delivery system. Int J Nanomedicine 14: 605-622.

Ayodeji ID, Schijven M, Jakimowicz J and Greve JW (2007) Face validation of the Simbionix LAP Mentor virtual reality training module and its applicability in the surgical curriculum. Surgical endoscopy 21: 1641-1649.

Banales JM, Huebert RC, Karlsen T, Strazzabosco M, LaRusso NF and Gores GJ (2019) Cholangiocyte pathobiology. Nat Rev Gastroenterol Hepatol 16: 269-281.

Bankir L, Bichet DG and Morgenthaler NG (2017) Vasopressin: physiology, assessment and osmosensation. J Intern Med 282: 284-297.

Bergquist A and von Seth E (2015) Epidemiology of cholangiocarcinoma. Best practice & research. Clinical gastroenterology 29: 221-232.

Birkmeyer JD, Stukel TA, Siewers AE, Goodney PP, Wennberg DE and Lucas FL (2003) Surgeon volume and operative mortality in the United States. New England Journal of Medicine 349: 2117-2127.

Bittner JG, Mellinger JD, Imam T, Schade RR and MacFadyen BV (2010) Face and construct validity of a computer-based virtual reality simulator for ERCP. Gastrointestinal endoscopy 71: 357-364.

Blidaru D, Blidaru M, Pop C, Crivii C and Seceleanu A (2010) The common bile duct: size, course, relations. Rom J Morphol Embryol 51: 141-144.

Bowman CE, Selen Alpergin ES, Cavagnini K, Smith DM, Scafidi S and Wolfgang MJ (2019) Maternal Lipid Metabolism Directs Fetal Liver Programming following Nutrient Stress. Cell Rep 29: 1299-1310 e1293.

Boyer JL (2013) Bile formation and secretion. Compr Physiol 3: 1035-1078.

Buzink SN, Christie LS, Goossens RH, de Ridder H and Jakimowicz JJ (2010) Influence of anatomic landmarks in the virtual environment on simulated angled laparoscope navigation. Surgical endoscopy 24: 2993-3001.

Cafarelli A, Miloro P, Verbeni A, Carbone M and Menciassi A (2016) Speed of sound in rubber-based materials for ultrasonic phantoms. Journal of ultrasound 19: 251-256.

Campisano S, La Colla A, Echarte SM and Chisari AN (2019) Interplay between early-life malnutrition, epigenetic modulation of the immune function and liver diseases. Nutr Res Rev 32: 128-145.

Cappell MS and Friedel DM (2019) Stricter national standards are required for credentialing of endoscopic-retrograde-cholangiopancreatography in the United States. World journal of gastroenterology 25: 3468-3483.

Carbone M, Condino S, Mattei L, Forte P, Ferrari V and Mosca F (Year) Anthropomorphic ultrasound elastography phantoms — Characterization of silicone materials to build breast elastography phantoms. 2012 Annual International Conference of the IEEE Engineering in Medicine and Biology Society pp 492-494.

Carter RF and Saypol GM (1952) Transabdominal cholangiography. J Am Med Assoc 148: 253-255.

Casciaro S, Conversano F, Musio S, Casciaro E, Demitri C and Sannino A (2009) Full experimental modelling of a liver tissue mimicking phantom for medical ultrasound studies employing different hydrogels. J Mater Sci Mater Med 20: 983-989.

Chavalitdhamrong D and Draganov PV (2012) Endoscopic ultrasound-guided biliary drainage. World journal of gastroenterology 18: 491-497.

Chiang JY (2013) Bile acid metabolism and signaling. Compr Physiol 3: 1191-1212.

Chiarelli P, Lanata A, Carbone M and Domenici C (2010) High frequency poroelastic waves in hydrogels. Journal of the Acoustical Society of America 127: 1197-1207.

Choi E, Adams F, Palagi S, Gengenbacher A, Schlager D, Muller PF, Gratzke C, Miernik A, Fischer P and Qiu T (2020) A High-Fidelity Phantom for the Simulation and Quantitative Evaluation of Transurethral Resection of the Prostate. Annals of biomedical engineering 48: 437-446.

Choi HJ, Moon JH, Ko BM, Hong SJ, Koo HC, Cheon YK, Cho YD, Lee JS, Lee MS and Shim CS (2009) Overtube-balloon-assisted direct peroral cholangioscopy by using an ultra-slim upper endoscope (with videos). Gastrointestinal endoscopy 69: 935-940.

Committee AT, Goodman AJ, Melson J, Aslanian HR, Bhutani MS, Krishnan K, Lichtenstein DR, Navaneethan U, Pannala R, Parsi MA, Schulman AR, Sethi A, Sullivan SA, Thosani N, Trikudanathan G, Trindade AJ, Watson RR and Maple JT (2019) Endoscopic simulators. Gastrointestinal endoscopy 90: 1-12.

Creswell CH, The Royal College of Surgeons of Edinburgh: historical notes from 1505 to 1905. Edinburgh (UK): Oliver and Boyd: 1926.

Culjat MO, Goldenberg D, Tewari P and Singh RS (2010) A REVIEW OF TISSUE SUBSTITUTES FOR ULTRASOUND IMAGING. Ultrasound in Medicine and Biology 36: 861-873.

Cuschieri A, Francis N, Crosby J and Hanna GB (2001) What do master surgeons think of surgical competence and revalidation? Am J Surg 182: 110-116.

D'Souza WD, Madsen EL, Unal O, Vigen KK, Frank GR and Thomadsen BR (2001a) Tissue mimicking materials for a multi-imaging modality prostate phantom. Medical Physics 28: 688-700.

D'Souza WD, Madsen EL, Unal O, Vigen KK, Frank GR and Thomadsen BR (2001b) Tissue mimicking materials for a multi-imaging modality prostate phantom. Med Phys 28: 688-700.

Davoodi E, Montazerian H, Khademhosseini A and Toyserkani E (2020) Sacrificial 3D printing of shrinkable silicone elastomers for enhanced feature resolution in flexible tissue scaffolds. Acta Biomater 117: 261-272.

Dawe SR, Windsor JA, Broeders JA, Cregan PC, Hewett PJ and Maddern GJ (2014) A systematic review of surgical skills transfer after simulation-based training: laparoscopic cholecystectomy and endoscopy. Ann Surg 259: 236-248.

Deng X, Zeng Z, Peng B, Yan S and Ke W (2018) Mechanical Properties Optimization of Poly-Ether-Ether-Ketone via Fused Deposition Modeling. Materials (Basel) 11.

Desilets DJ, Banerjee S, Barth BA, Kaul V, Kethu SR, Pedrosa MC, Pfau PR, Tokar JL, Varadarajulu S, Wang A, Song L, Rodriguez SA and Comm AT (2011) Endoscopic simulators. Gastrointestinal endoscopy 73: 861-867.

Desser TS (2007) Simulation-based training: the next revolution in radiology education? J Am Coll Radiol 4: 816-824.

Dhir V, Itoi T, Fockens P, Perez-Miranda M, Khashab MA, Seo DW, Yang AM, Lawrence KY and Maydeo A (2015) Novel ex vivo model for hands-on teaching of and training in EUS-guided biliary drainage: creation of "Mumbai EUS" stereolithography/3D printing bile duct prototype (with videos). Gastrointestinal endoscopy 81: 440-446.

Dietrich CF, Bibby E, Jenssen C, Saftoiu A, Iglesias-Garcia J and Havre RF (2018) EUS elastography: How to do it? Endosc Ultrasound 7: 20-28.

Dobson J and Walker RM, Barbers and Barber-Surgeons of London: A History of the Barbers' and Barber-Surgeons Companies. Oxford (UK): Blackwell Scientific Publications: 1979.

Dunnington GL (1996) The art of mentoring. Am J Surg 171: 604-607.

Ericsson KA, The acquisition of expert performance: An introduction to some of the issues. 1996; p 1-50.

Ericsson KA (2008) Deliberate Practice and Acquisition of Expert Performance: A General Overview. Academic Emergency Medicine 15: 988-994.

Everhart JE and Ruhl CE (2009) Burden of digestive diseases in the United States Part III: Liver, biliary tract, and pancreas. Gastroenterology 136: 1134-1144.

Falkenstein DB, Abrams RM, Kessler RE, Jones B, Johnson G and Zimmon DS (1974) ENDOSCOPIC RETROGRADE CHOLANGIOPANCREATOGRAPHY IN DOG - MODEL FOR TRAINING AND RESEARCH. Gastrointestinal endoscopy 21: 25-26.

Ferlitsch A, Glauninger P, Gupper A, Schillinger M, Haefner M, Gangl A and Schoefl R (2002) Evaluation of a virtual endoscopy simulator for training in gastrointestinal endoscopy. Endoscopy 34: 698-702.

Ferlitsch A, Schoefl R, Puespoek A, Miehsler W, Schoeniger-Hekele M, Hofer H, Gangl A and Homoncik M (2010) Effect of virtual endoscopy simulator training on performance of upper gastrointestinal endoscopy in patients: a randomized controlled trial. Endoscopy 42: 1049-1056.

Fong Y, Buell JF, Collins J, Martinie J, Bruns C, Tsung A, Clavien PA, Nachmany I, Edwin B, Pratschke J, Solomonov E, Koenigsrainer A and Giulianotti PC (2020) Applying the Delphi process for development of a hepatopancreaticobiliary robotic surgery training curriculum. Surgical endoscopy 34: 4233-4244.

Forte AE, Galvan S, Manieri F, Rodriguez y Baena F and Dini D (2016) A composite hydrogel for brain tissue phantoms. Materials & Design 112: 227-238.

Fortmeier D, Mastmeyer A, Schroder J and Handels H (2016) A Virtual Reality System for PTCD Simulation Using Direct Visuo-Haptic Rendering of Partially Segmented Image Data. IEEE J Biomed Health Inform 20: 355-366.

Franzese CB and Stringer SP (2007) The evolution of surgical training: perspectives on educational models from the past to the future. Otolaryngol Clin North Am 40: 1227-1235, vii.

Frimberger E, von Delius S, Rosch T, Karagianni A, Schmid RM and Prinz C (2008) A novel and practicable ERCP training system with simulated fluoroscopy. Endoscopy 40: 517-520.

Garbin N, Mamunes AP, Sohn D, Hawkins RW, Valdastri P and Obstein KL (2019) Evaluation of a novel low-cost disposable endoscope for visual assessment of the esophagus and stomach in an ex-vivo phantom model. Endoscopy international open 7: E1175-E1183.

Garcia-Cano J (2007) 200 supervised procedures: the minimum threshold number for competency in performing endoscopic retrograde cholangiopancreatography.

Surgical endoscopy 21: 1254-1255.

Gosline AH, Vasilyev NV, Butler EJ, Folk C, Cohen A, Chen R, Lang N, Del Nido PJ and Dupont PE (2012) Percutaneous intracardiac beating-heart surgery using metal MEMS tissue approximation tools. The International journal of robotics research 31: 1081-1093.

Graber MA, Wyatt C, Kasparek L and Xu YH (2005) Does simulator training for medical students change patient opinions and attitudes toward medical student procedures in the emergency department? Academic Emergency Medicine 12: 635-639.

Graham MF, Cooperberg PL, Cohen MM and Burhenne HJ (1980) The size of the normal common hepatic duct following cholecystectomy: an ultrasonographic study. Radiology 135: 137-139.

Grillo HC (1999) To impart this art: The development of graduate surgical education in the United States. Surgery 125: 1-14.

Groen AK, Bloks VW, Verkade H and Kuipers F (2014) Cross-talk between liver and intestine in control of cholesterol and energy homeostasis. Mol Aspects Med 37: 77-88.

Grund KE, Ingenpass R, Durst F, Schweizer U, Vietz M and Aurich V (2012) New Hands-on Simulator for Realistic Training of Diagnostic and Therapeutic ERCP. Endoskopie Heute 25: 14-17.

Halm EA, Lee C and Chassin MR (2002) Is volume related to outcome in health care? A systematic review and methodologic critique of the literature. Annals of Internal Medicine 137: 511-520.

Hamdorf JM and Hall JC (2000) Acquiring surgical skills. British Journal of Surgery 87: 28-37.

Hamilton EC, Scott DJ, Fleming JB, Rege RV, Laycock R, Bergen PC, Tesfay ST and Jones DB (2002) Comparison of video trainer and virtual reality training systems on acquisition of laparoscopic skills. Surgical endoscopy 16: 406-411.

Han Y, Glaser S, Meng F, Francis H, Marzioni M, McDaniel K, Alvaro D, Venter J, Carpino G, Onori P, Gaudio E, Alpini G and Franchitto A (2013) Recent advances in the morphological and functional heterogeneity of the biliary epithelium. Exp Biol Med (Maywood) 238: 549-565.

Heelan Gladden AA, Conzen KD, Benge MJ, Gralla J and Kennealey PT (2018) A Vascular Anastomosis Simulation Can Provide a Safe and Effective Environment for Resident Skills Development. J Surg Educ 75: 1367-1373.

Herreros de Tejada A (2014) ESD training: A challenging path to excellence. World J Gastrointest Endosc 6: 112-120.

Heymann F, Peusquens J, Ludwig-Portugall I, Kohlhepp M, Ergen C, Niemietz P, Martin C, van Rooijen N, Ochando JC, Randolph GJ, Luedde T, Ginhoux F, Kurts C, Trautwein C and Tacke F (2015) Liver inflammation abrogates immunological tolerance induced by Kupffer cells. Hepatology 62: 279-291.

Hiroyoshi J, Arita J, Gonoi W, Akamatsu N, Kaneko J and Hasegawa K (2019) Significance of Glisson's capsule invasion in patients with colorectal liver metastases undergoing resection. Am J Surg 218: 887-893.

Hoeffel C, Azizi L, Lewin M, Laurent V, Aube C, Arrive L and Tubiana JM (2006) Normal and pathologic features of the postoperative biliary tract at 3D MR cholangiopancreatography and MR imaging. Radiographics 26: 1603-1620.

Hohmann E, Brand JC, Rossi MJ and Lubowitz JH (2019) Proficiency-Based Training Using Simulator-Based Tools Could be Validated for Certification of Surgical Procedural Proficiency. Arthroscopy 35: 3167-3170.

Holt BA, Hearn G, Hawes R, Tharian B and Varadarajulu S (2015) Development and evaluation of a 3D printed endoscopic ampullectomy training model (with video). Gastrointestinal endoscopy 81: 1470-1475 e1475.

Huber T, Wunderling T, Paschold M, Lang H, Kneist W and Hansen C (2018) Highly immersive virtual reality laparoscopy simulation: development and future aspects.

International journal of computer assisted radiology and surgery 13: 281-290.

Hungr N, Long J-A, Beix V and Troccaz J (2012) A realistic deformable prostate phantom for multimodal imaging and needle-insertion procedures. Medical Physics 39: 2031-2041.

Hunt A, Ristolainen A, Ross P, Opik R, Krumme A and Kruusmaa M (2013) Low cost anatomically realistic renal biopsy phantoms for interventional radiology trainees. Eur J Radiol 82: 594-600.

Itoi T, Gotoda T, Baron TH, Sofuni A, Itokawa F, Tsuji S, Tsuchiya T, Tanaka R, Tonozuka R, Honjo M, Ryozawa S, Kawai T, Moriyasu F and Isayama H (2013) Creation of simulated papillae for endoscopic sphincterotomy and papillectomy training by using in vivo and ex vivo pig model. Gastrointestinal endoscopy 77: 793-800.

Itoi T, Moon JH and Waxman I (2011) Current status of direct peroral cholangioscopy. Dig Endosc 23 Suppl 1: 154-157.

James PD, Antonova L, Martel M and Barkun A (2016) Measures of trainee performance in advanced endoscopy: A systematic review. Best practice & research. Clinical gastroenterology 30: 421-452.

Javan R and Zeman MN (2018) A Prototype Educational Model for Hepatobiliary Interventions: Unveiling the Role of Graphic Designers in Medical 3D Printing. Journal of digital imaging 31: 133-143.

Jirapinyo P, Kumar N and Thompson CC (2015) Validation of an endoscopic part-task training box as a skill assessment tool. Gastrointestinal endoscopy 81: 967-973.

Jovanovic I, Fry LC, Rustemovic N, Bilic B, Ivekovic H, D'Assuncao M and Monkemuller K (2015) Initial validation of a simple, nonbiological, mechanical ERCP training model for cannulation and stent placement. Endoscopy 47 Suppl 1 UCTN: E585-586.

Jung Y, Kato M, Lee J, Gromski MA, Chuttani R and Matthes K (2013) Effectiveness of circumferential endoscopic mucosal resection with a novel tissue-anchoring device. World J Gastrointest Endosc 5: 275-280.

Kedia P, Gaidhane M and Kahaleh M (2013) Endoscopic guided biliary drainage: how can we achieve efficient biliary drainage? Clin Endosc 46: 543-551.

Kenngott HG, Wunscher JJ, Wagner M, Preukschas A, Wekerle AL, Neher P, Suwelack S, Speidel S, Nickel F, Oladokun D, Albala L, Maier-Hein L, Dillmann R, Meinzer HP and Muller-Stich BP (2015) OpenHELP (Heidelberg laparoscopy phantom): development of an open-source surgical evaluation and training tool. Surgical endoscopy 29: 3338-3347.

Khan R, Plahouras J, Johnston BC, Scaffidi MA, Grover SC and Walsh CM (2018) Virtual reality simulation training for health professions trainees in gastrointestinal endoscopy. The Cochrane database of systematic reviews 8: CD008237.

Khan R, Plahouras J, Johnston BC, Scaffidi MA, Grover SC and Walsh CM (2019) Virtual reality simulation training in endoscopy: a Cochrane review and meta-analysis. Endoscopy 51: 653-664.

King N, Kunac A, Johnsen E, Gallina G and Merchant AM (2016) Design and validation of a cost-effective physical endoscopic simulator for fundamentals of endoscopic surgery training. Surgical endoscopy 30: 4871-4879.

Koch AD, Ekkelenkamp VE, Haringsma J, Schoon EJ, de Man RA and Kuipers EJ (2015) Simulated colonoscopy training leads to improved performance during patient-based assessment. Gastrointestinal endoscopy 81: 630-636.

Kong X, Nie L, Zhang H, Wang Z, Ye Q, Tang L, Huang W and Li J (2016) Do 3D Printing Models Improve Anatomical Teaching About Hepatic Segments to Medical Students? A Randomized Controlled Study. World journal of surgery 40: 1969-1976.

Kotsis SV and Chung KC (2013) Application of the "see one, do one, teach one" concept in surgical training. Plast Reconstr Surg 131: 1194-1201.

Kowalski T, Kanchana T and Pungpapong S (2003) Perceptions of gastroenterology fellows regarding ERCP competency and training. Gastrointestinal endoscopy 58: 345-349.

Kozarek RA (2017) The future of ERCP. Endoscopy international open 5: E272-E274.

Kunert W, Land C, Braun M, Reichold J, Kirschniak A and Falch C (2020) The impact of guided instrument insertion during laparoscopy: a randomized study with novices in an optical box trainer. Surgical endoscopy 34: 787-795.

Kunkler K (2006) The role of medical simulation: an overview. International Journal of Medical Robotics and Computer Assisted Surgery 2: 203-210.

Lal BK, Jordan W, Kashyap VS, Kwolek CJ, Moore WS, Mukherjee D and Schermerhorn ML (2020) Clinical competence statement of the Society for Vascular Surgery on training and credentialing for transcarotid artery revascularization. J Vasc Surg 72: 779-789.

Larghi A and Waxman I (2006) Endoscopic direct cholangioscopy by using an ultra-slim upper endoscope: a feasibility study. Gastrointestinal endoscopy 63: 853-857.

Laugier R and Grandval P (2011) Endoscopic retrograde cholangiopancreatography. Endoscopy 43: 990-992.

Lee H, Jang EJ, Kim GH, Yi NJ, Kim DH, Yoo S, Row HS, Jung CW, Oh SY and Ryu HG (2019) Effect of Case Volume on Mortality After Pediatric Liver Transplantation in Korea. Transplantation 103: 1649-1654.

Lee TH, Choi JH, Lee SS, Cho HD, Seo DW, Park SH, Lee SK, Kim MH and Park DH (2014) A pilot proof-of-concept study of a modified device for one-step endoscopic ultrasound-guided biliary drainage in a new experimental biliary dilatation animal model. World journal of gastroenterology 20: 5859-5866.

Lei C and Palm K, Crisis Resource Management Training in Medical Simulation. In StatPearls, Treasure Island (FL), 2021.

Leung J, Lim B, Ngo C, Lao WC, Wing LY, Hung I, Li M and Leung FW (2012a) Head-To-Head Comparison of Practice With Endoscopic Retrograde Cholangiopancreatography Computer And Mechanical Simulators By Experienced Endoscopists And Trainees. Digestive Endoscopy 24: 175-181.

Leung JW, Lee JG, Rojany M, Wilson R and Leung FW (2007) Development of a novel ERCP mechanical simulator. Gastrointestinal endoscopy 65: 1056-1062.

Leung JW and Yen D (2011) ERCP training - the potential role of simulation practice. Journal of interventional gastroenterology 1: 14-18.

Leung JW, Yen DC, Brian SL and Leung FW (2012b) Didactic teaching and simulator practice improve trainees' understanding and performance of biliary papillotomy. Journal of interventional gastroenterology 3: 64-68.

Liao WC, Leung JW, Wang HP, Chang WH, Chu CH, Lin JT, Wilson RE, Lim BS and Leung FW (2013) Coached practice using ERCP mechanical simulator improves trainees' ERCP performance: a randomized controlled trial. Endoscopy 45: 799-805.

Lim BS, Leung JW, Lee J, Yen D, Beckett L, Tancredi D and Leung FW (2011) Effect of ERCP Mechanical Simulator (EMS) Practice on Trainees' ERCP Performance in the Early Learning Period: US Multicenter Randomized Controlled Trial. American Journal of Gastroenterology 106: 300-306.

Lin CC, Chen CJ, Chu CH, Hung CY, Chen MJ, Wang HY, Shih SC and Liu CY (2012) Evaluating the feasibility of direct peroral cholangioscopy training with an endoscopic simulator. Dig Dis Sci 57: 2016-2021.

Lin HH, Lonic D and Lo LJ (2018) 3D printing in orthognathic surgery - A literature review. J Formos Med Assoc 117: 547-558.

Liu H, Zhang H, Han W, Lin H, Li R, Zhu J and Huang W (2021) 3D Printed Flexible Strain Sensors: From Printing to Devices and Signals. Adv Mater 33: e2004782.

Lowther M and Armstrong B, Roles and Responsibilities of a Simulation Technician. In

StatPearls, Treasure Island (FL), 2021.

Lv Y, Lau WY, Wu H, Chang S, NingLiu, Li Y and Deng J (2015) Etiological Causes of Intrahepatic and Extrahepatic Bile Duct Dilatation. International Journal of New Technology and Research 1: 53-57.

Madsen EL, Hobson MA, Shi HR, Varghese T and Frank GR (2005) Tissue-mimicking agar/gelatin materials for use in heterogeneous elastography phantoms. Physics in Medicine and Biology 50: 5597-5618.

Madsen EL, Zagzebski JA, Banjavie RA and Jutila RE (1978) Tissue Mimicking Materials For Ultrasound Phantoms. Medical Physics (Woodbury) 5: 391-394.

Madurska MJ, Poyade M, Eason D, Rea P and Watson AJ (2017) Development of a Patient-Specific 3D-Printed Liver Model for Preoperative Planning. Surgical innovation 24: 145-150.

Maggi LE, Krüger MAv, Pereira WCA and Monteiro EEC, Development of silicon-based materials for ultrasound biological phantoms. In 2009 IEEE International Ultrasonics Symposium, 2009; pp 1962–1965.

Majno G, The healing hand: man and wound in the ancient world. Cambridge (MA): Harvard University Press: 1975.

Manuel B, Valcke M, Keygnaert I and Roelens K (2021) Improving medical students' communication competencies to deal with intimate partner violence using clinical simulations in Mozambique. BMC Med Educ 21: 126.

Manzanares MA, Solanas M, Moral R, Escrich R, Vela E, Costa I and Escrich E (2015) Dietary extra-virgin olive oil and corn oil differentially modulate the mRNA expression of xenobiotic-metabolizing enzymes in the liver and in the mammary gland in a rat chemically induced breast cancer model. Eur J Cancer Prev 24: 215-222.

Mashiko T, Otani K, Kawano R, Konno T, Kaneko N, Ito Y and Watanabe E (2015) Development of three-dimensional hollow elastic model for cerebral aneurysm clipping simulation enabling rapid and low cost prototyping. World Neurosurg 83: 351-361.

Matsumoto ED, Hamstra SJ, Radomski SB and Cusimano MD (2001) A novel approach to endourological training: training at the Surgical Skills Center. J Urol 166: 1261-1266.

Matteotti R (2019) Robotic surgery for liver, pancreas, and bile duct pathologies: A critical analysis and personal views. International Journal of Gastrointestinal Intervention 8: 6-9.

McGaghie WC, Issenberg SB, Cohen ER, Barsuk JH and Wayne DB (2011) Does Simulation-Based Medical Education With Deliberate Practice Yield Better Results Than Traditional Clinical Education? A Meta-Analytic Comparative Review of the Evidence. Academic Medicine 86: 706-711.

Miller AT, Safranski DL, Wood C, Guldberg RE and Gall K (2017) Deformation and fatigue of tough 3D printed elastomer scaffolds processed by fused deposition modeling and continuous liquid interface production. J Mech Behav Biomed Mater 75: 1-13.

Minaga K and Kitano M (2018) Recent advances in endoscopic ultrasound-guided biliary drainage. Dig Endosc 30: 38-47.

Minaga K, Kitano M, Gon C, Yamao K, Imai H, Miyata T, Kamata K, Omoto S, Takenaka M and Kudo M (2017) Endoscopic ultrasonography-guided choledochoduodenostomy using a newly designed laser-cut metal stent: Feasibility study in a porcine model. Dig Endosc 29: 211-217.

Moon JH, Ko BM, Choi HJ, Hong SJ, Cheon YK, Cho YD, Lee JS, Lee MS and Shim CS (2009) Intraductal balloon-guided direct peroral cholangioscopy with an ultraslim upper endoscope (with videos). Gastrointestinal endoscopy 70: 297-302.

Mu C and Zhu W (2019) Antibiotic effects on gut microbiota, metabolism, and beyond. Appl Microbiol Biotechnol 103: 9277-9285.

Muavha DA, Ras L and Jeffery S (2019) Laparoscopic surgical anatomy for pelvic floor surgery. Best Pract Res Clin Obstet Gynaecol 54: 89-102.

Mukai S, Itoi T, Baron TH, Takada T, Strasberg SM, Pitt HA, Ukai T, Shikata S, Teoh AYB, Kim MH, Kiriyama S, Mori Y, Miura F, Chen MF, Lau WY, Wada K, Supe AN, Gimenez ME, Yoshida M, Mayumi T, Hirata K, Sumiyama Y, Inui K and Yamamoto M (2017) Indications and techniques of biliary drainage for acute cholangitis in updated Tokyo Guidelines 2018. Journal of hepato-biliary-pancreatic sciences 24: 537-549.

Nakagaki BN, Mafra K, de Carvalho E, Lopes ME, Carvalho-Gontijo R, de Castro-Oliveira HM, Campolina-Silva GH, de Miranda CDM, Antunes MM, Silva ACC, Diniz AB, Alvarenga DM, Lopes MAF, de Souza Lacerda VA, Mattos MS, Araujo AM, Vidigal PVT, Lima CX, Mahecha GAB, Madeira MFM, Fernandes GR, Nogueira RF, Moreira TG, David BA, Rezende RM and Menezes GB (2018) Immune and metabolic shifts during neonatal development reprogram liver identity and function. J Hepatol 69: 1294-1307.

Nguyen L, Brunicardi FC, DiBardino DJ, Scott BG, Awad SS, Bush RL and Brandt ML (2006) Education of the modern surgical resident: Novel approaches to learning in the era of the 80-hour workweek. World journal of surgery 30: 1120-1127.

NIH_Consensus (2002) NIH state-of-the-science statement on endoscopic retrograde cholangiopancreatography (ERCP) for diagnosis and therapy. NIH consensus and state-of-the-science statements 19: 1-26.

Ogura T and Higuchi K (2016) A review of treatment options for bile duct stones. Expert Rev Gastroenterol Hepatol 10: 1271-1278.

Ookhtens M and Kaplowitz N (1998) Role of the liver in interorgan homeostasis of glutathione and cyst(e)ine. Semin Liver Dis 18: 313-329.

Ostergaard ML, Ewertsen C, Konge L, Albrecht-Beste E and Bachmann Nielsen M (2016) Simulation-Based Abdominal Ultrasound Training - A Systematic Review. Ultraschall Med 37: 253-261.

Ozer MA, Uguz A, Unalp OV, Coker A, Govsa F, Guler E, Bati AH and Pinar Y (2021) Perceptions of porta-celiac vascular models for hepatic surgery and their use in residency training. Surg Radiol Anat.

Pacioni A, Carbone M, Freschi C, Viglialoro R, Ferrari V and Ferrari M (2015) Patient-specific ultrasound liver phantom: materials and fabrication method. International journal of computer assisted radiology and surgery 10: 1065-1075.

Palter VN, Grantcharov T, Harvey A and Macrae HM (2011) Ex vivo technical skills training transfers to the operating room and enhances cognitive learning: a randomized controlled trial. Ann Surg 253: 886-889.

Papanikolaou IS, van der Voort IR, Chopra SS, Seebauer CJ, Rump J, Papas MG, Triantafyllou K, Baumgart DC, Teichgraber UK, Wiedenmann B and Rosch T (2014) MRI-guided percutaneous transhepatic cholangiodrainage: feasibility study in a porcine model. Scand J Gastroenterol 49: 722-726.

Parra-Blanco A, Gonzalez N, Gonzalez R, Ortiz-Fernandez-Sordo J and Ordieres C (2013) Animal models for endoscopic training: do we really need them? Endoscopy 45: 478-484.

Parsi MA (2011) Peroral cholangioscopy in the new millennium. World journal of gastroenterology 17: 1-6.

Parulekar SG (1989) Sonography of the distal cystic duct. J Ultrasound Med 8: 367-373.

Pimpin L, Cortez-Pinto H, Negro F, Corbould E, Lazarus JV, Webber L, Sheron N and Committee EHS (2018) Burden of liver disease in Europe: Epidemiology and analysis of risk factors to identify prevention policies. J Hepatol 69: 718-735.

Popa CC, Marinescu AA, Mohan AG, Saceleanu MV and Ciurea AV (2018) Remember: Ambroise Pare (1510-1590) - message for young surgeons. Rom J Morphol Embryol 59: 637-640.

Radosa C, Schaab F, Hofmockel T, Kuhn JP and Hoffmann RT (2019) [Percutaneous biliary and gallbladder interventions]. Radiologe 59: 342-347.

Rankin JS (2006) William Stewart Halsted - A lecture by Dr. Peter D. Olch. Annals of Surgery 243: 418-425.

Robert M and Zollinger J, Atlas of surgical operations. New York: Macmillan: 1983.

Roh S, Parekh DP, Bharti B, Stoyanov SD and Velev OD (2017) 3D Printing by Multiphase Silicone/Water Capillary Inks. Adv Mater 29.

Rossi UG, Rutigliani M and DeCensi A (2019) Hepatobiliary and Pancreatic: Sub-Glisson's capsule hepatic multiple nodular formations. J Gastroenterol Hepatol 34: 1132.

Rui M, Lee JE, Vauthey JN and Conrad C (2018) Enhancing surgical performance by adopting expert musicians' practice and performance strategies. Surgery 163: 894-900.

Sachdeva AK (2011) Credentialing of surgical skills centers. Surgeon 9 Suppl 1: S19-20.

Sarmah P, Voss J, Ho A, Veneziano D and Somani B (2017) Low vs. high fidelity: the importance of 'realism' in the simulation of a stone treatment procedure. Curr Opin Urol 27: 316-322.

Schuberth OO and Sjogren SE (2010) On Cholangiography. Acta Radiologica 22: 780-795.

Schulte SJ, Baron RL, Teefey SA, Rohrmann CA, Jr., Freeny PC, Shuman WP and Foster MA (1990) CT of the extrahepatic bile ducts: wall thickness and contrast enhancement in normal and abnormal ducts. AJR Am J Roentgenol 154: 79-85.

Shah J and Darzi A (2001) Surgical skills assessment: an ongoing debate. BJU Int 88: 655-660.

Shaharan S and Neary P (2014) Evaluation of surgical training in the era of simulation. World J Gastrointest Endosc 6: 436-447.

Shanmugan S, Leblanc F, Senagore AJ, Ellis CN, Stein SL, Khan S, Delaney CP and Champagne BJ (2014) Virtual reality simulator training for laparoscopic colectomy: what metrics have construct validity? Dis Colon Rectum 57: 210-214.

Sica A, Invernizzi P and Mantovani A (2014) Macrophage plasticity and polarization in liver homeostasis and pathology. Hepatology 59: 2034-2042.

Singh S, Sedlack RE and Cook DA (2014) Effects of simulation-based training in gastrointestinal endoscopy: a systematic review and meta-analysis. Clin Gastroenterol Hepatol 12: 1611-1623 e1614.

Sosa JA, Bowman HM, Gordon TA, Bass EB, Yeo CJ, Lillemoe KD, Pitt HA, Tielsch JM and Cameron JL (1998) Importance of hospital volume in the overall management of pancreatic cancer. Annals of Surgery 228: 429-436.

Stavrakis AI, Ituarte PHG, Ko CY and Yeh MW (2007) Surgeon volume as a predictor of outcomes in inpatient and outpatient endocrine surgery. Surgery 142: 887-894.

Sujka JA, Safcsak K, Bhullar IS and Havron WS, 3rd (2018) Simulation-Based Testing of Pager Interruptions During Laparoscopic Cholecystectomy. J Surg Educ 75: 1351-1356.

Sureka B, Bansal K, Patidar Y and Arora A (2016) Magnetic resonance cholangiographic evaluation of intrahepatic and extrahepatic bile duct variations. The Indian journal of radiology & imaging 26: 22-32.

Tamada K, Tomiyama T, Oohashi A, Aizawa T, Nishizono T, Wada S, Tano S, Miyata T, Satoh Y, Ido K and Kimura K (1999) Bile duct wall thickness measured by intraductal US in patients who have not undergone previous biliary drainage. Gastrointestinal endoscopy 49: 199-203.

Tan X, Li D, Jeong M, Yu T, Ma Z, Afat S, Grund KE and Qiu T (2021) Soft Liver Phantom with a Hollow Biliary System. Annals of biomedical engineering.

Tang R, Ma L, Li A, Yu L, Rong Z, Zhang X, Xiang C, Liao H and Dong J (2018) Choledochoscopic Examination of a 3-Dimensional Printing Model Using Augmented Reality Techniques: A Preliminary Proof of Concept Study. Surgical

innovation 25: 492-498.

Tedesco MM, Pak JJ, Harris EJ, Jr., Krummel TM, Dalman RL and Lee JT (2008) Simulation-based endovascular skills assessment: the future of credentialing? J Vasc Surg 47: 1008-1001; discussion 1014.

Thompson CM, Saad NE, Quazi RR, Darcy MD, Picus DD and Menias CO (2013) Management of iatrogenic bile duct injuries: role of the interventional radiologist. Radiographics 33: 117-134.

Thomson JE, Van Dijk SM, Brand M, Van Santvoort HC and Besselink MG (2018) Managing Infected Pancreatic Necrosis. Chirurgia (Bucur) 113: 291-299.

Trefts E, Gannon M and Wasserman DH (2017) The liver. Curr Biol 27: R1147-R1151.

Turner MA and Fulcher AS (2001) The cystic duct: normal anatomy and disease processes. Radiographics 21: 3-22; questionnaire 288-294.

Turney BW (2014) A new model with an anatomically accurate human renal collecting system for training in fluoroscopy-guided percutaneous nephrolithotomy access. J Endourol 28: 360-363.

van der Wiel SE, Kuttner Magalhaes R, Rocha Goncalves CR, Dinis-Ribeiro M, Bruno MJ and Koch AD (2016) Simulator training in gastrointestinal endoscopy - From basic training to advanced endoscopic procedures. Best practice & research. Clinical gastroenterology 30: 375-387.

van Noort R (2012) The future of dental devices is digital. Dent Mater 28: 3-12.

Vardevanyan H, Holzinger J and Forstner R (2017) Hepatoduodenal lymph node metastasis mimicking Klatskin tumor in a patient with sigmoid colon mucinous cancer. Radiology case reports 12: 494-499.

Velazquez-Avina J, Sobrino-Cossio S, Chavez-Vargas C, Sulbaran M and Monkemuller K (2014) Development of a novel and simple ex vivo biologic ERCP training model. Gastrointestinal endoscopy 80: 1161-1167.

Von Delius S, Thies P, Meining A, Wagenpfeil S, Burian M, Huber W, Weidenbach H, Ebert MP, Neu B, Ludwig L, Almeida J, Prinz C, Schmid RM and Frimberger E (2009) Validation of the X-Vision ERCP Training System and Technical Challenges During Early Training of Sphincterotomy. Clinical Gastroenterology and Hepatology 7: 389-396.

Walter AJ (2006) Surgical education for the twenty-first century: Beyond the apprentice model. Obstetrics and Gynecology Clinics of North America 33: 233-236.

Wang L, Zhou D, Hou H, Wu C and Geng X (2018) Application of "three lines and one plane" as anatomic landmarks in laparoscopic surgery for bile duct stones. Medicine (Baltimore) 97: e0155.

Wanjek C, Bad medicine : misconceptions and misuses revealed, from distance healing to vitamin O. John Wiley and Sons, Inc.: 2003.

Waschke KA and Coyle W (2018) Advances and Challenges in Endoscopic Training. Gastroenterology 154: 1985-1992.

Waxman I, Dillon T, Chmura K, Wardrip C, Chennat J and Konda V (2010) Feasibility of a novel system for intraductal balloon-anchored direct peroral cholangioscopy and endotherapy with an ultraslim endoscope (with videos). Gastrointestinal endoscopy 72: 1052-1056.

Wissamitanan T, Dechwayukul C, Kalkornsurapranee E and Thongruang W (2020) Proper Blends of Biodegradable Polycaprolactone and Natural Rubber for 3D Printing. Polymers (Basel) 12.

Wynn G, Lykoudis P and Berlingieri P (2018) Development and implementation of a virtual reality laparoscopic colorectal training curriculum. Am J Surg 216: 610-617.

Xiang L, Li J, Wang Q, Tang R and Qi J (2018) Leptin Gene Transfer Improves Symptoms of Type 2 Diabetic Mice by Regulating Leptin Signaling Pathway and Insulin Resistance of Peripheral Tissues. Hum Gene Ther 29: 68-76.

Yang Y, Zhou Z, Liu R, Chen L, Xiang H and Chen N (2018) Application of 3D visualization and 3D printing technology on ERCP for patients with hilar cholangiocarcinoma. Experimental and therapeutic medicine 15: 3259-3264.

Yao R, Yang Y, Lian S, Shi H, Liu P, Liu Y, Yang H and Li S (2018) Effects of Acute Cold Stress on Liver O-GlcNAcylation and Glycometabolism in Mice. Int J Mol Sci 19.

Yiannakopoulou E, Nikiteas N, Perrea D and Tsigris C (2015) Virtual reality simulators and training in laparoscopic surgery. Int J Surg 13: 60-64.

Yokoda RT and Carey EJ (2019) Primary Biliary Cholangitis and Primary Sclerosing Cholangitis. Am J Gastroenterol 114: 1593-1605.

Young S, The annals of the barber-surgeons of London, from their records and other source. London: Blade, East & Blades: 1890.

Zammit D, Safran T, Ponnudurai N, Jaberi M, Chen L, Noel G and Gilardino MS (2020) Step-Specific Simulation: The Utility of 3D Printing for the Fabrication of a Low-Cost, Learning Needs-Based Rhinoplasty Simulator. Aesthet Surg J 40: NP340-NP345.

Zell K, Sperl JI, Vogel MW, Niessner R and Haisch C (2007) Acoustical properties of selected tissue phantom materials for ultrasound imaging. Physics in Medicine and Biology 52: N475-N484.

Zheng JP, Li CZ and Chen GQ (2019) Multimaterial and multicolor 3D-printed model in training of transnasal endoscopic surgery for pituitary adenoma. Neurosurg Focus 47: E21.

Żmudzińska M, Inglot M, Zaleska-Dorobisz U, Jankowski L and Swiatek-Najwer E (2018) The assessment of the applicability of shear wave elastography in modelling of the mechanical parameters of the liver. Acta of Bioengineering and Biomechanics 20: 59-64.

8. Declaration on contributions

The work was partly conducted in Eberhard Karl University of Tübingen, Max-Planck Institute for Intelligent Systems, and University of Stuttgart under the supervision of Prof. Dr. K.E Grund, Dr. D.Wichmann, and Dr. T Qiu.

The 3D digital models of the biliary tree and liver were designed by M. Jeong, who works at University of Stuttgart as a Ph.D. candidate. I was partly involved as a medical consultant.

The fabrication of the liver phantom was partly assisted by D. Li, who works at Max-Planck Institute for Intelligent system.

The programming work for the quantitative assessment system was carried out by Dr. T Qiu using the Arduino integrated development environment (IDE, Arduino, Italy).

The CT scan of the liver phantom was performed by Dr. S. Afat.

X. Tan, D. Li, M. Jeong, T. Yu, Z. Ma, S. Afat, K-E Grund, T. Qiu, D. Wichmann, and A. Königsrainer contribute to the proof reading for the publication and the dissertation.

All other experiments, figures and tables, and the statistical analysis were carried out independently by me, with the training of Dr. T Qiu.

I hereby declare that I wrote this dissertation on my own and I have not used any other source and aids than quoted.

Tübingen, 10.03.2021

Xiangzhou Tan

9. Publication

Results of this thesis were partially published in the following publication:

Title:

Soft Liver Phantom with a Hollow Biliary System

Authors:
Xiangzhou Tan, Dandan Li, Moonkwang Jeong, Tingting Yu, Zhichao Ma, Saif Afat, Karl-Ernst Grund, and Tian Qiu.

Journal:
Annals of Biomedical Engineering.

Cite:
Tan X, Li D, Jeong M, Yu T, Ma Z, Afat S, Grund KE, Qiu T. Soft Liver Phantom with a Hollow Biliary System. Ann Biomed Eng. 2021 Feb 16. doi: 10.1007/s10439-021-02726-x. Epub ahead of print. PMID: 33594636.

10. <u>Acknowledgements</u>